CAPITAL UNIVERSITY OF SCIENCE AND TECHNOLOGY, ISLAMABAD

Sensors and Internal Fault Detection and Isolation for Lithium-ion Batteries using Structural Analysis

by

Naima Nageen

A thesis submitted in partial fulfillment for the degree of Master of Science

in the

Faculty of Engineering
Department of Electrical Engineering

2019

To my beloved Parents and my brothers Mateen Ilyas and Tauseeq Ilyas.

CERTIFICATE OF APPROVAL

Sensors and Internal Fault Detection and Isolation for Lithium-ion Batteries using Structural Analysis

by

Naima Nageen

(MEE171017)

THESIS EXAMINING COMMITTEE

S. No.	Examiner	Name	Organization
(a)	External Examiner	Dr. Muhammad Abid	PIEAS, Islamabad
(b)	Internal Examiner	Dr. Fazal ur Rehman	CUST, Islamabad
(c)	Supervisor	Dr. Aamer Iqbal Bhatti	CUST, Islamabad

Dr. Aamer Iqbal Bhatti
Thesis Supervisor
October, 2019

Dr. Noor Muhammad Khan
Head
Dept. of Electrical Engineering
October, 2019

Dr. Imtiaz Ahmad Taj
Dean
Faculty of Engineering
October, 2019

Author's Declaration

I, **Naima Nageen** hereby state that my MS thesis titled "**Sensors and Internal Fault Detection and Isolation for Lithium-ion Batteries using Structural Analysis**" is my own work and has not been submitted previously by me for taking any degree from Capital University of Science and Technology, Islamabad or anywhere else in the country/abroad.

At any time if my statement is found to be incorrect even after my graduation, the University has the right to withdraw my MS Degree.

(Naima Nageen)
Registration No: MEE171017

Plagiarism Undertaking

I solemnly declare that research work presented in this thesis titled "**Sensors and Internal Fault Detection and Isolation for Lithium-ion Batteries using Structural Analysis**" is solely my research work with no significant contribution from any other person. Small contribution/help wherever taken has been dully acknowledged and that complete thesis has been written by me.

I understand the zero tolerance policy of the HEC and Capital University of Science and Technology towards plagiarism. Therefore, I as an author of the above titled thesis declare that no portion of my thesis has been plagiarized and any material used as reference is properly referred/cited.

I undertake that if I am found guilty of any formal plagiarism in the above titled thesis even after award of MS Degree, the University reserves the right to withdraw/revoke my MS degree and that HEC and the University have the right to publish my name on the HEC/University website on which names of students are placed who submitted plagiarized work.

(Naima Nageen)
Registration No: MEE171017

Acknowledgements

After being grateful to Almighty Allah who gave me strength and courage to complete my research work, I would like to express an immense gratitude towards **Dr. Aamer Iqbal Bhatti**, who is not only my supervisor but also my mentor. This research work would not have completed without his guidance and support. I am fortunate to work with him. His strong command on my area of research and extra-ordinary problem solving skills are the key factors in completion of this thesis.

I would also like to thank every single member at CASPR Lab with special thanks to Farhan Hanif and Zohaib Latif who always helped me to get through my queries related to my research work.

It would be an ultimate pleasure to acknowledge my Parents, who taught me the patience, devotion and commitment and always supported me during thick and thin and encouraged me to stay motivated throughout my degree program in order to achieve my goals.

Lastly, i would like to thank my friends Sidra Ghayour and Faryal Akbar for always being there whenever i needed them for help.

(Naima Nageen)
Registration No: MEE171017

Abstract

Li-ion batteries are attracting a lot of attention because these are one of the most advanced rechargeable batteries that have been extensively used for many past years. The beneficial performance in terms of high power, high energy density and long life cycle has gained high consideration for the Li-ion battery technology. Electronic devices such as laptop computers and mobile phones use these energy storage systems as their source of power. These batteries have also been used in electric vehicles (EVs) such as cars, passenger aircrafts and unmanned aerial vehicles (UAVs).

To assure the best performance and safety and to minimize the effect of aging, battery sensors and internal fault diagnosis is very important. This work represents a model-based fault diagnosis technique for a lithium-ion battery to detect and isolate the faults of current sensor, voltage sensor, increase in the internal resistance and decrease in the total amount of available Li-ions inside the battery.

In this work Dulmage-Mendelsohn (DM) decomposition has been performed to check the detectability of all the model faults. A group of sensors is added in the battery model to achieve maximum fault isolability with the help of sensor placement analysis. Then Minimal Structurally Over-determined (MSO) sets are identified to generate four residuals. For the purpose of residual generation, concepts from observer-based techniques are utilized. The proposed FDI scheme has been verified using simulations in MATLAB Simulink.

Contents

List of Figures

List of Tables

Abbreviations

ARR	Analytical Redundancy Relation
CVs	Control Volumes
CC	Constant Current
CV	Constant Voltage
EKF	Extended Kalman Filter
EOD	End of Discharge
EV	Electric Vehicles
FD	Fault Detection
FDI	Fault Detection and Isolation
FI	Fault Isolation
LCO	Lithium Cobalt Oxide
LIB	Lithium Ion Battery
SA	Structural Analysis
SEI	Solid-electrolyte Interface
SOC	State of Charge
UAVs	Unmanned Aerial Vehicles

Symbols

U_o	Reference Potential
T	Electrode Temperature
R	Universal Gas Constant
n	number of electrons transferred in the reaction
F	Faraday's Constant
J_i	Current Density
J_{i0}	Exchange Current Density
τ	Empirical Time Constant
$V_{INT,i}$	Activity Correction Term
k_i	Lumped Parameter of Contants
V_{U_i}	Equilibrium Potential
V_o	Ohmic Overpotential
V_{η_i}	Surface Overpotential
c_{b_i}	Concentration of the Charge on Bulk Volume
c_{s_i}	Concentration of the Charge on Surface Volume
q^{max}	Total amount of available charge in a battery cell
q_p	Amount of available charge on positive electrode
q_n	Amount of available charge on negative electrode
x_{s_i}	Mole Fraction on the surface of respective i^{th} electrode

Chapter 1

Introduction

1.1 Background

Since the new and upcoming technologies are in dire need of higher capacity, more compact, rechargeable, safe batteries, therefore Prof.Goodenough, an American physicist [1] conceived a new idea in 1980. To create a type of lithium battery, in which the lithium (Li) could travel as a Li^+ ion from one electrode to the other through the battery. Since lithium had one of the largest electrochemical potentials and it was one of the lightest periodic table element, thats why this combination managed to produce some of the highest possible voltages in the lightest and utmost compact volumes.

In the year 1991, the first Li-ion battery was commercialized by Sony Corp. The growth of Li-ion battery technology did not stopped here because these batteries provided high energy density, design flexibility, low maintenance cost and highest available voltage than other battery technologies.

Li-ion batteries, are attracting a lot of attention because they are one of the most advanced rechargeable batteries. In the previous decade, compared with nickel metal-hydride and lead-acid batteries [2, 3], its beneficial performance in

terms of power, energy and life cycle has earned considerably high attention for the technology of the Li-ion battery. Electrical and electronic devices like laptop computers and mobile phones which are portable as well, use these energy storage systems as their source of power [4]. These batteries have also been extensively used in electric vehicles (EVs) such as cars, passenger aircrafts and unmanned aerial vehicles (UAVs).

Due to huge number of requests from the electric-power vehicles, the demand for Li-ion batteries has increased significantly [5]. According to the estimates, electric-powered vehicles share about 50% of the total sales with the consumer uses, and both of these sectors need almost 100 GW-hours of Liion batteries by 2018. In addition, the fluctuating and intermittent supply from the renewable green energy resources such as solar or wind can be buffered by using the Li-ion batteries to even out the difference between energy demand and supply i.e during the daytime surplus solar energy can be produced and stored in Li-ion batteries, which can later be used to supply energy when the sunlight is not available at night.

1.2 Basic Structure of Lithium-ion Batteries

In a Li- ion cell, cathode and anode (negative electrode) are contacted by the electrolyte which consists of Li-ions. A separator which is typically a microporous polymer membrane is used to isolate the electrodes from each other, which stops the electrons but allows Li-ions to be exchanged between the electrodes. Preserved chemical energy is released due to electrochemical reactions at the two electrodes [4]. Ceramic, Polymer and Gel electrolyte, in addition to the liquid electrolyte, were also investigated for applications in Li-ion batteries.

Fundamental operating principle of a normal Li-ion battery cell is presented in Figure. 1.1. The primary design of those cells, which commercialized by Sony two

decades ago, is followed in Li-ion cells today, while many types of electrode materials, separators, and electrolyte were investigated. Mostly the economic cells are fabricated in discharged state. Typically used cathodes (e.g., $LiCoO_2$, $LiFePO_4$) and anodes (e.g., carbon, lithiated carbon), while in their discharged state can be managed easily during industrial experiments and they are stable in atmosphere.

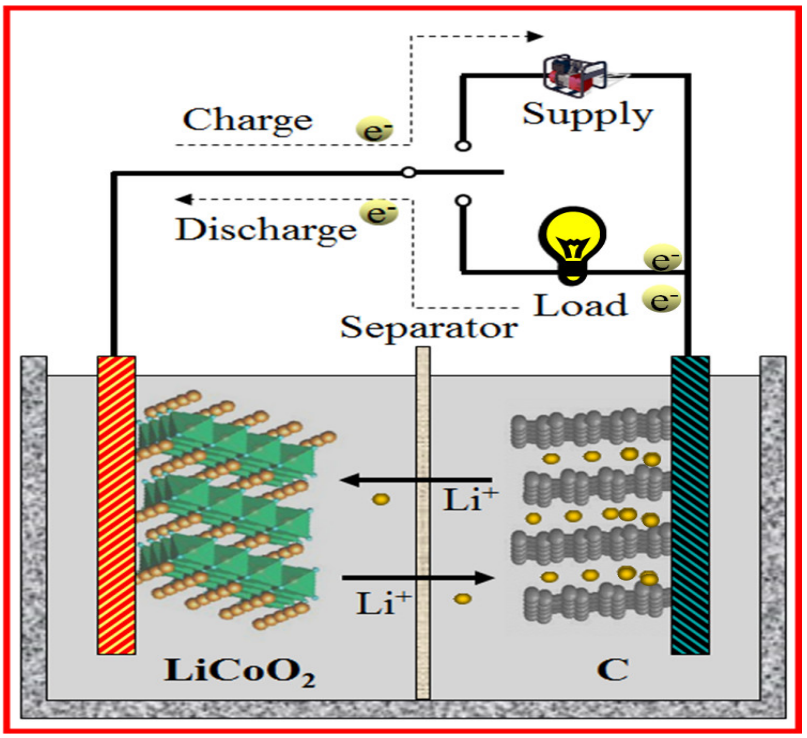

FIGURE 1.1: The basic components and operation of a Li- ion battery cell [4].

1.3 Why Li-ion Batteries are Preferred

A Li-ion battery has many advantages [6]. These advantages include:

1.3.1 High Energy Density

The major advantage of the Li-ion battery technology is that its energy density is higher than other existing battery technologies. Its always needed to produce the batteries with much higher density because they support the electronic devices such as mobile phones [6], which can consume more power and still operate for

longer hours between charges. Furthermore, the power tools and electric-powered vehicles can also be included as power applications. Higher power density is a distinct advantage provided by the lithium ion batteries. The battery system with a really high energy density can benefit electric vehicles [7]. In Figure. 1.2 comparison of different rechargeable batteries has been shown.

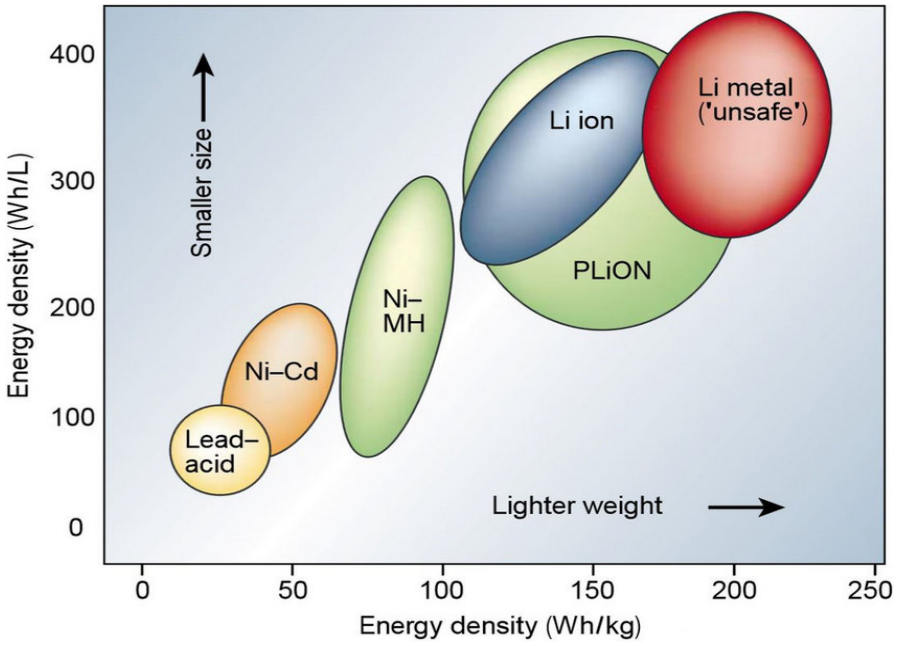

FIGURE 1.2: Energy densities and specific energy comparison of different battery technologies. [7]

1.3.2 Low Self Discharge

The biggest issue with many battery technologies is their rate of self-discharge. The amount of self-discharge for other battery cells such as NiMH and Ni-Cad forms is much higher than the lithium-ion cells. After being charged within first 4 hours, it is typically around 5% but then reduces to almost 1 or 2% per month.

1.3.3 Low Maintenance

Li-ion battery does not need a lot of maintenance like other rechargeable batteries, to ensure their good performance which is a major advantage. To safeguard that they dont exhibit the memory effect, Ni-Cad cells required a periodic discharge.

The Li-ion cells do not need these maintenance methods, because this does not affect Li-ion cells.

1.3.4 No Need for Priming

Some batteries that are rechargeable, on their first charge, need priming. Li-ion cells and batteries dont require these methods.

1.3.5 Light Weight and Easy Installation

$LiFePO_4$ and LCO batteries are typically half the mass of lead-acid batteries reducing concerns about battery weight and provide more energy. Lithium provides the same or even greater energy at half the size and weight compared to the other battery chemistries. This ensures easier installation and design flexibility.

1.3.6 Quick Charging

Time taken by the Lithium-ion batteries to charge is a fraction of the time taken by other batteries. These batteries are preferred over the others for this reason, especially in gadgets and other devices that require frequent charging.

1.4 Constraints of Li-ion Batteries

The major constraints of Li-ion batteries are:

1.4.1 Cost

Cost is a major lithium ion battery limitation. Manufacturing them can cost 40% than Nickel cadmium cells. Their usage in mass produced consumer items makes their cost a major factor where any extra costs are a vital issue.

1.4.2 Low Thermal Stability

Whenever, beyond a certain point, a lithium metal oxide cathode is heated, it results in exothermic release of oxygen, in which the cell can burst into flames due to the start of a runaway reaction [8].

1.4.3 Protection Required

Unlike other rechargeable technologies, Li-ion batteries are not as strong. These batteries need to be protected from over charging and discharging too far. Furthermore, safe limits are set in which their current has to be maintained. The disadvantage of a Li-ion battery is that these batteries require protection circuitry like Battery Management System, to work in a proper safe operating limits. With modern integrated circuit technology′s help, if the battery is not interchangeable then this can be easily integrated within the equipment or into the battery. Incorporation of the Battery Management System enables Li-ion batteries to be used without any special knowledge. The supply to the battery will be cut by charger after the battery is fully charged, which enables them to be left on charge for longer durations [8].

1.4.4 Aging

Li-ion battery suffers from aging which is one of the major consumer electronics disadvantage [9, 10]. This figure is improving as the lithium-ion technology progresses, if batteries are embedded in the equipment then it can be a big issue because after a while, batteries may need to be replaced.

A typical lithium cobalt oxide (LCO) battery meant for consumers has to be partially charged (40% to 50%) and should be stored in a cold storage area whenever needed [11]. The battery life will increase by storing it under these conditions and low temperatures.

1.5 Battery Modelling Methodologies

Several battery modelling methodologies have been established. Generally, the classifications of those models can be empirical models, electrochemical engineering models, multi-physics models, and molecular/atomist models [12].

1.5.1 Empirical Models

Empirical models do not use any physicochemical principles and are totally established on applying certain functions to past experimental data [13]. A popular form of the empirical models can be electrical circuit equivalent models [14].

1.5.2 Electrochemical Engineering Models

These models which basically include electrochemical, transport and kinetics phenomenon, are continuum models [15–18]. The advantages of former type of model are being computationally efficient and their disadvantage is limited accuracy and robustness. They cannot represent aging well due to the approximations in battery behaviour that are made. The advantage for the latter type of model is that they are very accurate, but they are computationally inefficient, which makes them ill-suited to online application of prognostics because complex sets of partial differential equations have to be solved to use them.

1.5.3 Multi-physics Models

Multi-physics models [19] are less suited to online application of prognostics due to limited accuracy and robustness.

1.5.4 Atomist Models

Atomist models are not robust and even less suited to online application [12].

1.6 Relevant Physical Aging Mechanisms

Some relevant physical mechanisms that cause aging in the LIB are:

1.6.1 Growth of Solid-electrolyte Interface (SEI) Layer

With the growth of SEI layer [20, 21], negative electrode degrades, resulting in capacity loss. Internal resistance increases due to the decay of electrolyte and the development of the SEI layer [11]. During cycling and storage at high temperatures, these layers are formed and entrain the lithium.

1.6.2 Lithium Corrosion

Lithium(Li) which is present in the negative electrode of active carbon material, corrodes with the passage of time and it leads to deterioration. The irreversible loss of lithium-ions which are mobile, causes the decrease in capacity.

1.6.3 Lithium Plating

The lithium faces an irreversible loss because a plating layer forms on the negative electrode at high charge rates, low cell voltages and low temperatures.

1.6.4 Contact Loss

An increase in impedance and contact loss is caused when the SEI layer [20] is disconnected from the negative electrode. Due to increased electrolyte resistance and the catalytic evolution of the SEI layer on graphite anode, this increased interfacial resistance is the main source for power fade [22]. Figure. 1.3 shows how a LIB degrades due to physical aging mechanisms. In the Figure. 1.4 Cause and effects of aging mechanisms has been shown in detail.

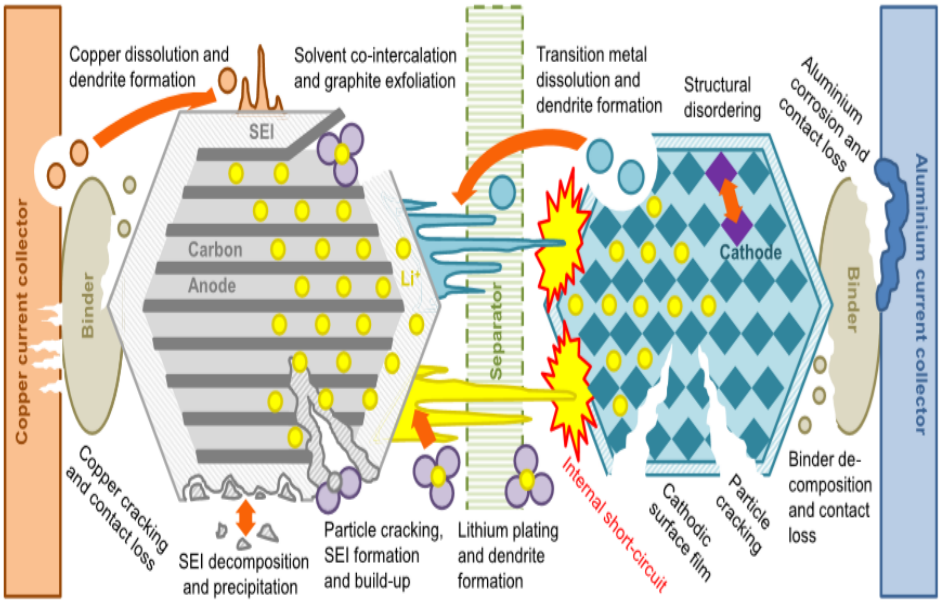

FIGURE 1.3: Physical aging mechanisms in the electrodes [23].

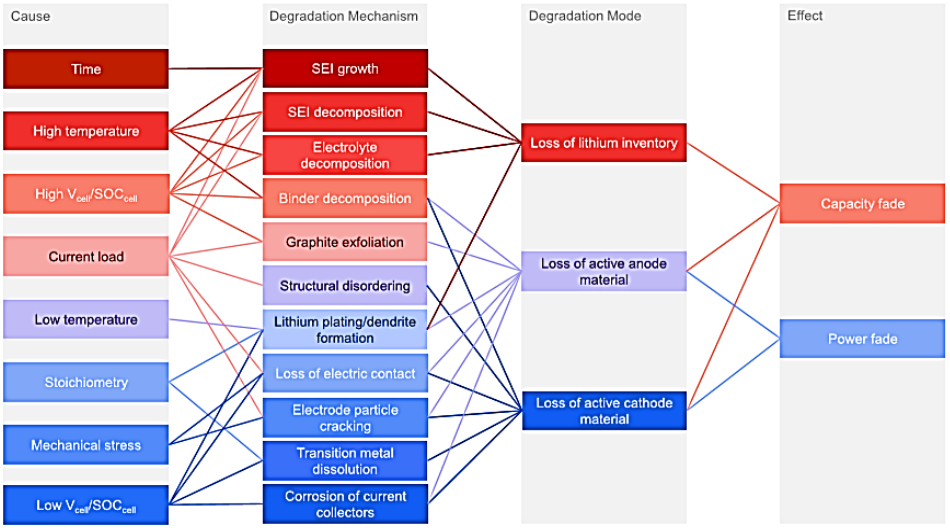

FIGURE 1.4: Cause and effect of degradation mechanisms and associated degradation modes [23]

1.7 Thesis Organization

The thesis contains five chapters along with introduction.

Chapter 2: This chapter includes literature survey of aging factors in LIBs. Further, some Fault diagnostic techniques presented by different researchers to detect various types of faults in LIBs have also been discussed. Also, Structural Analysis

theory and the work done in this field by researchers is presented.

Chapter 3: This chapter consists of mathematical modeling of LIB system. This chapter also provides necessary information regarding FDI scheme using SA. FDI scheme has been discussed briefly.

Chapter 4: This chapter comprises of results and simulations. The objective of fault isolation has been achieved using Sensor Placement Analysis. Also the residuals sensitive to each fault have also been designed.

Chapter 5: This chapter includes the final conclusion and some suggestions that can be adopted to extend this work in the future.

Chapter 2

Literature Survey

2.1 LIB Aging in the Literature

Aging is caused by degradation of Li ion cells. Due to the increasing usage of Li-ion batteries in demanding applications and their requirement to have a very long life sometimes exceeding more than 15 years, aging is becoming a big concern. Therefore to make correct life predictions, the knowledge about the capacity or power loss due to the side reactions is mandatory [24]. Due to their exposure to environmental circumstances and their usage, lithium ion (Li-ion) cells suffer degradation [9, 23, 25]. The cells ability to meet the power demands or store energy gets affected due to this degradation which leads to their end of life.

In [26] it is observed that the increase in internal resistance and capacity degradation are main contributors to aging. It has also been observed that due to the loss of mainly cyclible and active lithium ions, the degradation occurs [27].

Furthermore, the major fading mechanisms are the decline of the electrolyte conductivity and the growth of SEI layer [20]. With the help of a particle model, numerically and through experimental data, Zhang and White have also confirmed

these results [28]. The conclusion of their analysis was that the battery degradation, as a function of the operational temperature, varies non-linearly.

An analysis performed by [29] concluded that the side reactions that occur at anode due to decay of the solvent can be cause of the capacity fade at elevated operational temperatures, therefore it leads to SEI layer growth. The side reactions at the anode side are more prominent than at the cathode side. It is concluded that for long lifetime of the battery, it should be preserved in the most perfect conditions where the increase of internal resistance and capacity fade are small [11].

To estimate the above issue, both studied parameters (internal resistance and capacity fade) should be included, because this is an appropriate method.

Following are some of the main degradation factors:

2.1.1 Higher Temperature and Higher SOC

The market currently has various types of storage systems for the rechargeable energy, designed to offer specific applications and uses, but none can fulfil all of the demands.

The environmental conditions like higher operating temperature and higher SOC strongly affect the performance of lithium-ion batteries [11], affecting cycling behaviour. Due to the anode decomposition and growth of SEI layer, the side reactions result in increased internal resistance and capacity losses. Temperature and other operational conditions influences the nonlinear phenomena, which makes an impact on reduction of the battery lifetime and aging degradation. It has been observed that compared to the lower temperatures, the capacity deterioration is significantly high at higher operational temperatures (e.g., 60 and 40 C).

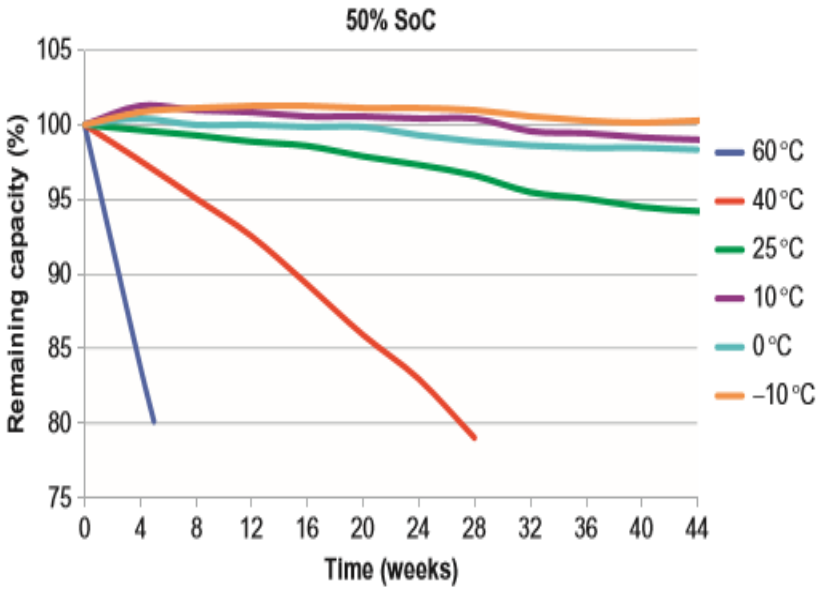

FIGURE 2.1: Capacity degradation at different temperatures and 50% SOC [11].

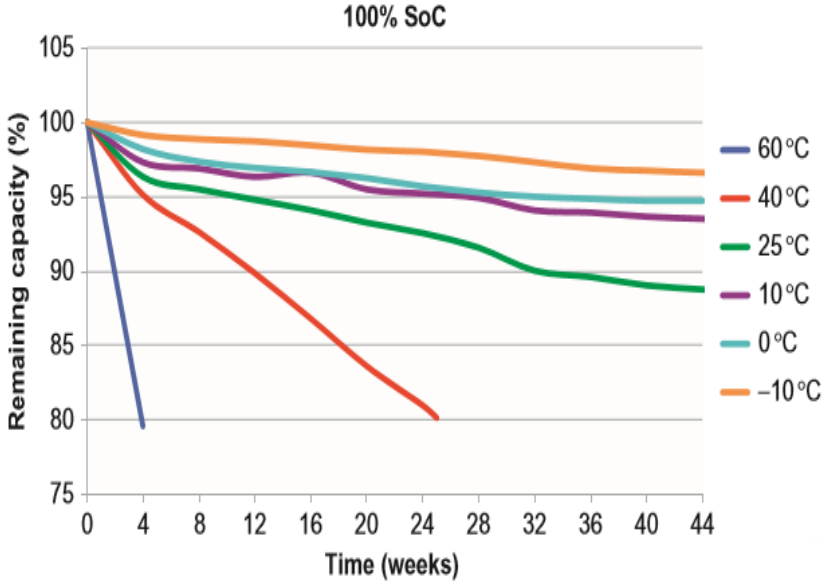

FIGURE 2.2: Capacity degradation at different temperatures and 100% SOC [11].

2.1.2 Cut-off Voltages and Charging Rates

Increase of internal resistance and capacity degradation are the long-term effects of cut-off voltages and charging current rates. It has been analysed that a critical charging cut-off voltage as well as a critical charging current exists [9]. Speed

of battery degradation accelerates greatly when the charging stress goes beyond the critical value. It is indicated that to retard battery degradation, the cut-off voltage and charging current should be reduced after a certain extent of battery degradation.

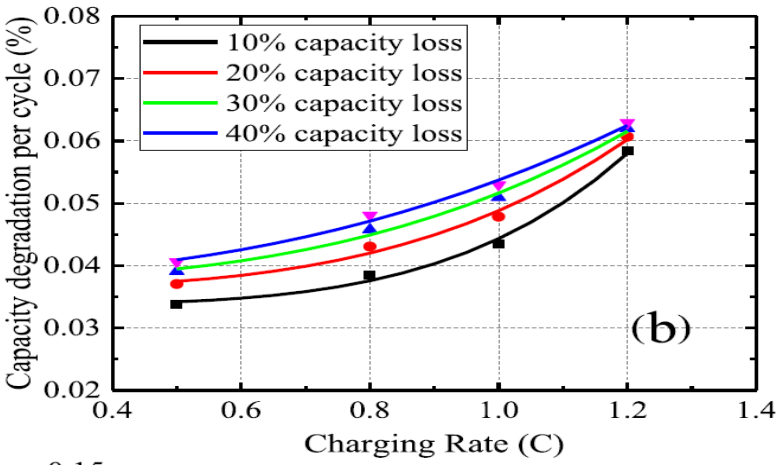

FIGURE 2.3: Degradation of capacity at different Charging Rates [9].

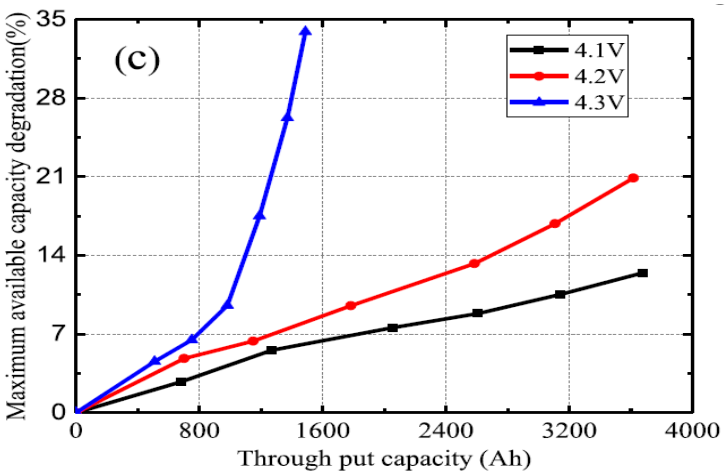

FIGURE 2.4: Degradation of capacity at different Cut-off Voltages [9].

2.1.3 Self Discharge

Self-discharge in lithium-ion batteries occur due to the high external temperatures, SEI formation and the loss of the active lithium ions [20, 23]. Loss in the overall power and Capacity degradation is caused by self-discharge of Li-ion batteries.

2.1.4 Cycling Rate and Cycle Number Effect

In the literature it has been described that further capacity fade occurs due to the cycling rate being fast which leads to accelerated aging, while greater capacity (lesser capacity fade) can be attributed to slower cycling rates [10, 25]. Similarly, due to the cycle aging, maximum storage capacity declines gradually and the battery capacity gets reduced with the greater number of cycles. The individual or combination of each of these: SEI layer establishment on the surfaces of current collectors and electrodes, active materials dissolution, electrolyte decomposition, structural changes of the electrodes and phase transitions in the insertion electrode contains the capacity loss traces due to the cycle aging, which are irreversible. It can be seen in the first step that during first 500 cycles the capacity fade is linear as represented in Figure. 2.5. In this step, the SEI film forms on the surfaces of electrode due to parasitic reactions, which causes lithium inventory loss and then the capacity fading arises. During the charging regime, the negative electrode gets fewer Li^+ as a subsequent implication. In the second step, interfacial kinetics gets restrained because the electrode surfaces have the SEI layer, due to which electrodes suffer the active material loss and therefore it increases the capacity fading.

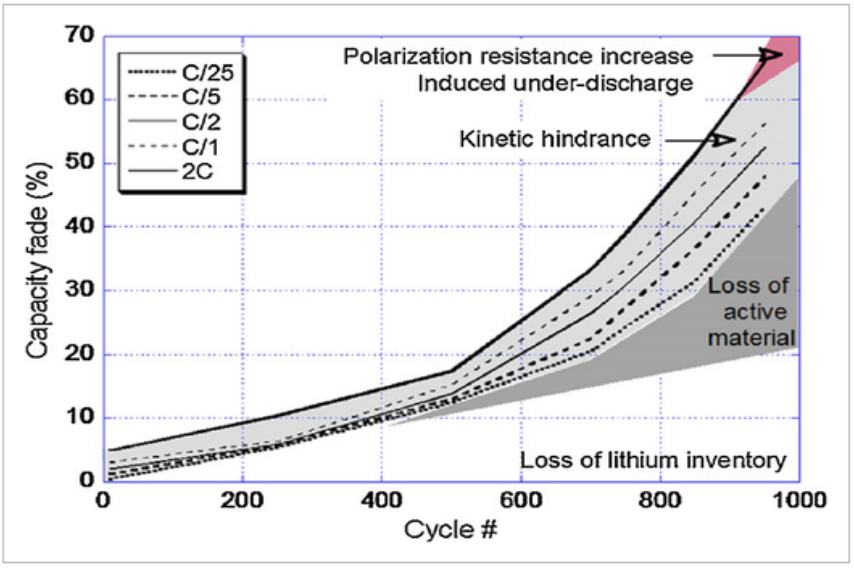

FIGURE 2.5: At various Crates, the cell capacity loss under room temperature as a function of cycle aging [25].

2.2 Fault Detection and Isolation

2.2.1 What is Fault and why FD and FI is Important

Manufacturing systems which comprises of different transportation system, robots and machine tools, have to fully satisfy their requirements so that the high-quality production can be completely efficient. The performance and availability of a whole system gets affected due to faults in a single component, therefore it can be said that the function of complex and huge electrical and transportation systems have big impacts on everyday life [30].

A *fault* is the occurrence of an undesirable event, that changes the behaviour of the electrical system in such a manner that the system is unable to serve its purpose. It may be caused by systems internal event, which creates a pipe leakage, stoppage of power supply or broken information link.

An ambient temperature increase can be caused by a change in environmental conditions which can eventually stop or even destroy the reactor. A human operator may bring the system out of its vital operation point by inputting a wrong control action. When a system gets back into its operation point, the performance gets considerably reduced due to an undetected design error. In any case, loss of functions or system performance gets degraded due to the parameter or system structure changes primarily caused by the faults.

Faults have to be found and decisions should be taken on time to stop their effects from spreading as soon as possible, so that damage to humans or machines and deteriorations of production can be avoided [30].

To make system fault tolerant, control equipment should carry out these measures. If these measures are effective, system functions will be fulfilled and the control algorithm will adapt to the faulty plant, after the performance is degraded

for a short time due to the fault.

In the Figure. 2.6 below it is clearly shown that how faulty plant is operated so that spread of system fault could be stopped in a reasonable amount of time.

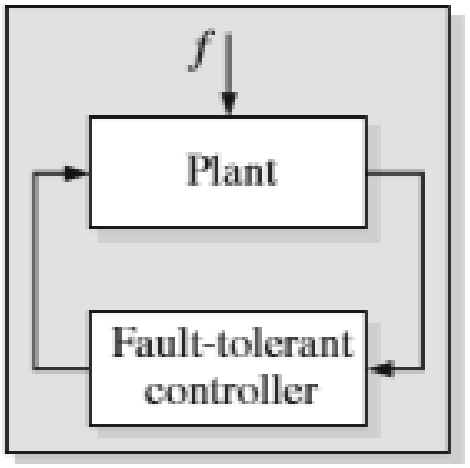

FIGURE 2.6: Fault-tolerant Control [30]

2.2.2 Fault Diagnosis Methods in the Literature

Fault diagnosis is to calculate the size of fault, confirm the location and its time of occurrence. *Fault detection* FD is the discovery of fault. Likewise, *Fault isolation* is confirmation of kind, time of detection and the separation of that specific fault from other system faults.

The field of Li-ion battery fault diagnosis is broad and in the literature there are many available methods found.

Much research has been done in the field of the battery fault diagnosis. Some of them are described below with their pros and cons.

2.2.2.1 Reduced Order Luenberger Observers Based Fault Diagnosis Scheme

In three-cell battery strings, for a single fault to be isolated, stock of reduced order Luenberger observers were used [31], and the major problem with this observer was that with measurement noise in a system, satisfactory performance cannot be achieved by it.

2.2.2.2 Non-linear Parity Equation based Fault Diagnosis Scheme

In the simulation environment to detect the fault of current or voltage sensor, the diagnostic method based on non-linear parity equation was applied under the assumption that temperature sensor does not contain any fault, and this sensor is working perfectly fine [32].

2.2.2.3 Multiple Model Based Fault Diagnosis Scheme

For the detection of over-charging and over-discharging in Li-ion batteries, multiple model-based diagnostic method was introduced, accompanying the complexity of identifying various models and difficulty in running many EKFs [33].

2.2.3 Importance of Battery Sensor FD and FI

The battery safety, performance, life and reliability can be guaranteed by the battery sensor FD and FI. The FDI system is required for the estimations of SOC and State of Health SOH, decrease in total available lithium ions, an increase in internal impedance and overcurrent, and over/undervoltage protection. These complex functions usually depend on resistance, voltage, current and total amount of available lithium ions sensor measurements. These sensors could be faulty due

to external shocks or manufacturing flaws [34]. If the sensor of current or voltage becomes defective due to any reason then the performance of estimating SoC and SoH would be deteriorated and the aging process would accelerate because the battery suffers from overcharge and overdischarge [10, 11, 24].

2.3 Structural Analysis Theory

2.3.1 Introduction

To resolve the complex fault diagnosis issues, another model-based methodology, structural analysis (SA) was introduced. The theory of SA is derived from the conception of the bond graph [35]. The SA theory was represented in [36] to analyze the fault isolability for the DAMADICS valve benchmark model, where it was proved that SA is an efcient way to rapidly evaluate the FI for a complicated system. The SA theory in a large and nonlinear model was also applied in [37] to obtain an optimal sensor placement scheme for maximal capability of FD and FI. The application of SA to design a diagnostic strategy was employed in [38] to detect and isolate different faults for the pack of lithium-ion battery. The SA method to implement a health monitoring scheme was also represented in [39] for an automated manual transmission (AMT), where the FD and FI are easily obtained with available set of sensors, and then a robust FDI system was efficiently designed. Based on the above introduction of SA theory, it is known that SA is an effective method of fault diagnosis on mechanical and controlling systems, and it has an eminent advantage of easily performing FD and FI analysis and realizing an efficient FDI method design for a complicated system.

2.3.2 Importance of Structural Analysis

To isolate and detect faults in a system, the fault diagnosis using SA is employed. Fault diagnosis has become really necessary due to the increased demand for reliability and safety of technical systems. One approach can be used where a set

of residuals can be generated and the different subsets of faults will be responded by different subsets of residuals. Decoupling the faults in those residuals is fundamental for this very reason. In addition, to handle the unknown inputs or disturbances, decoupling can also be used. Due to its insensitivity to the disturbances of a system and capability of detecting and isolating the faults in a close-loop system, model-based fault diagnosis can often be used even without requiring knowledge of system model parameters. After the identification algorithms, state observers and analytical redundant relations (ARR) are applied, a significant step of model-based fault diagnosis, residual generation can commonly be reached [40]. Structural analysis has an advantage that by representing a system defined by a set of algebraic and differential equations in a graphical way, the redundant part can easily be found. Furthermore, to isolate and detect faults, it can be used without having accurate system parameters knowledge [30].

2.3.3 FD and FI for LIB in the Literature

In [38] for the detection and isolation of faults in current, voltage temperature and cooling system, a systematic scheme has been presented using SA for the stock of Li-ion battery. Using SA, sequential residual generation based on ARR has been used in this work.

In [41] Battery system hazard analysis has been observed and the most compelling faults that were considered, are; temperature, voltage, current sensors, cooling system and the terminal connector faults.

In [42] isolate and detect the temperature sensor, voltage and current fault, a model-based systematic fault diagnosis scheme was presented. This scheme depends on sequential residual generation which uses statistical inference residual evaluation and SA theory. But lithium-ion battery aging effect was not considered in this work.

2.4 Gap Analysis

Many research has been done regarding battery fault diagnosis but these fault diagnosis schemes had their limitations with respect to FD and FI.

Structure analysis (SA) is an efficient fault diagnosis scheme and takes less computational effort. It is a kind of model-based technique, which depends on the mathematical model of the system. Its virtue is to execute a quick and efficient analysis of FD and FI with respect to the considered faults in system. An approach based on Analytical Redundant Relation (ARR), structural analysis for FDI presents the structure of a system on the basis of mathematical model that shows analytical redundancy and monitorable part of system is identified to extract the equations used for the detection and isolation of the faults later. SA has an advantage of representing the system described by a set of algebraic and differential equations in the form of a graph, redundant part can be found and then used to detect and isolate faults without having any accurate knowledge about system parameters. In SA methods, to further improve isolability properties of faults, it is also possible for the sensors to be placed.

Although much research has been done on the sensor and internal fault detection and isolation using SA of Lithium-ion batteries but there is not even a single literature found which discusses the battery aging parameters (increase in internal resistance and loss of available lithium-ions) with it. This work is an attempt to fill this gap by providing an efficient fault diagnosis scheme using SA, which not only detect these faults but also isolate them from each other.

2.5 Problem Statement

To design an efficient fault detection and Isolation (FDI) scheme using SA that can easily detect and isolate Lithium-ion battery current and voltage sensor, increase in internal resistance and loss of available active lithium-ions, faults by just relying

on the information about the battery dynamics and without having the accurate knowledge of battery parameters.

Chapter 3

System Modeling

3.1 Introduction

In this chapter the lithium-ion Battery Model [43] is described in detail involving the summary of Battery voltages.Then the Fault diagnostic scheme using SA for the battery sensor and internal fault detection and fault isolation has been discussed briefly.

3.2 Lithium-ion Battery Model

3.2.1 Symbolic Representation of Li-ion Battery

In Li-ion batteries chemical energy is converted in electrical energy, and usually contains multiple cells. The cell is made up of a +ve electrode and a -ve electrode with some amount of electrolyte in which the ions can move. For a Li-ion battery, mostly positive electrode consists of lithium cobalt oxide Li_xCoO_2 and negative electrode of lithiated carbon (Li_xC). At both ends of the cell, these materials are joined to metal-foil current collectors and unaccompanied by the microporous polymer separator film in which Li-ions can easily migrate. The electrolyte allows Li^+ to move within both electrodes. Ions enter or leave the material depending

upon the type of the respective electrode and even if the operation is battery charge or discharge.

During the process of charging, the -ve electrode (behaves as anode) contain high concentration of Li and have low potential. The cathode (+ve electrode) contain low concentration of Li and have high potential.

When electrodes are connected by an external load, electrons migrate automatically from the anode, tend to increase its potential, via load to the cathode, decreasing its potential, hence decreasing the overall cell voltage. Li-ions are concurrently transferred by the electrolyte from the anode, via separator, towards the cathode to conserve charge neutrality.

3.2.2 During Discharging

Illustration of the LIB during the discharge process is represented in Fig. 3.1.

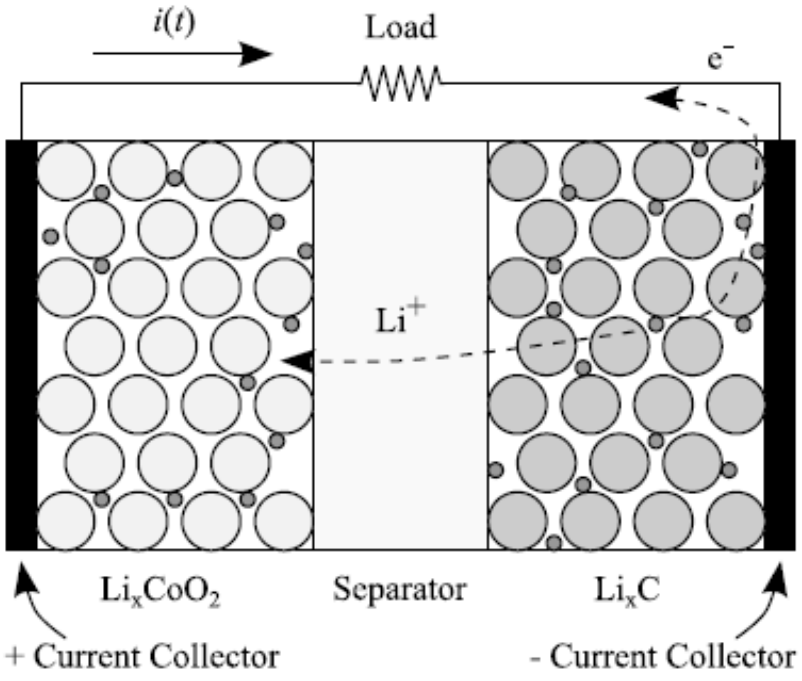

FIGURE 3.1: LIB during Discharging [43]

When the battery is completely charged, active Li-ions stay in the -ve electrode. As soon as the load is connected to the battery, current starts flowing towards -ve electrode from +ve electrode. The process is oxidation reaction in which dissipation of electrons happens in the -ve electrode (behaving like anode).

$$\mathrm{Li_xC} \xrightarrow{\text{discharging}} \mathrm{C} + \mathrm{xLi^+} + \mathrm{xe^-}$$

that causes the deliverance of electrons and Li-ions. These e^-s travel via load to +ve electrode from the negative electrode and the ions of lithium proceed in the same direction by the -ve electrode towards the +ve electrode across separator. Reduction reaction (i.e gain of electrons) takes place in the +ve electrode(behaving as cathode).

$$\mathrm{Li_{1-x}CoO_2} + \mathrm{xLi^+} + \mathrm{xe^-} \xrightarrow{\text{discharging}} \mathrm{LiCoO_2}$$

3.2.3 During Charging

During the procedure of charging, a source of current compels it to pass from -ve to the +ve electrode, this operation is given in Fig. 3.2.

During the procedure of charging, the material in the +ve electrode (behaving as the anode) gets oxidized. Li-ions are extracted as given in the following chemical reaction.

$$\mathrm{LiCoO_2} \xrightarrow{\text{charging}} \mathrm{Li_{1-x}CoO_2} + \mathrm{xLi^+} + \mathrm{xe^-}$$

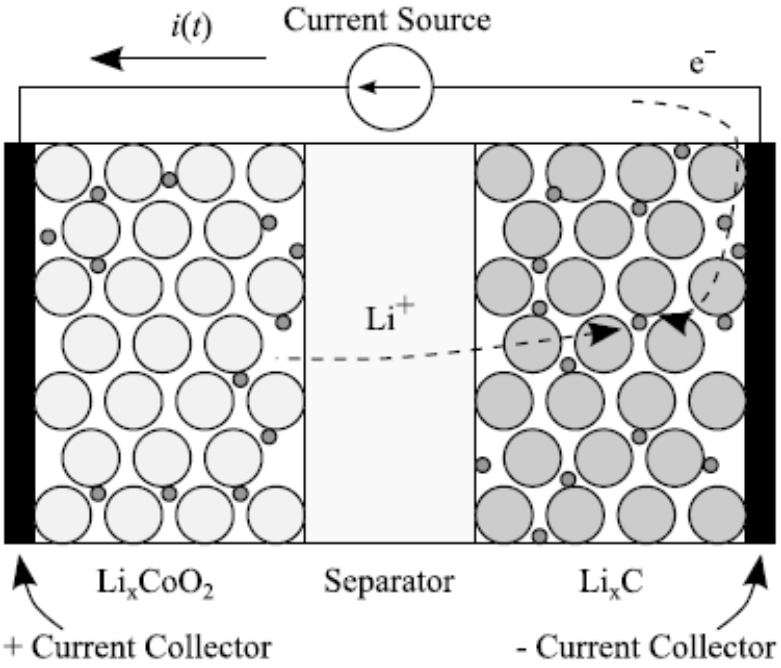

FIGURE 3.2: LIB during Charging [43]

which causes the dissipation of electrons and Li-ions, that can then travel towards the -ve electrode (behaving like cathode). Following reduction reaction occurs in -ve electrode:

$$C + xLi^{+} + xe^{-} \xrightarrow{\text{charging}} Li_xC$$

3.3 Battery Voltages

There are many electrochemical processes which are responsible for cells potential. In this work 18650 Li-ion batteries with a 4.2V nominal voltage and 2200mAh capacity will be focused.

LIB battery voltages are given in Fig. 3.3. The terminal voltage of the LIB $V(t)$ is actually the contrast among the potential at +ve current collector, $\phi_s(0,t)$, and -ve current collector, $\phi_s(L,t)$, without considering the dissipation of resistance in the current collectors (that are not presented in the diagram).

In the Figure. 3.3, the potentials changes with the distance $d \in [0, L]$, since the dissipation differs through the current collectors with the variation in the distance [43].

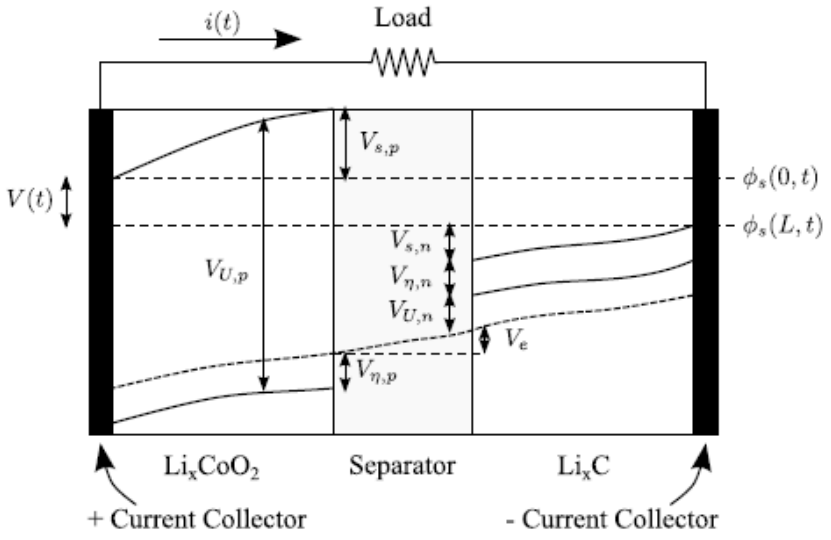

FIGURE 3.3: The Battery Voltages [43]

Different voltage terms are used to define the potentials at the current collectors. Equilibrium potential V_{U-p} is on the +ve current collector. Here voltage V_{U-p} is decreased by V_{s-p}, because of the surface overpotential and solid-phase ohmic resistance. Then the ohmic resistance of electrolyte makes another decrease in voltage V_e.

On the -ve electrode, there is a reduction in voltage, $V_{\eta-n}$ because of surface overpotential, and a decrease of voltage V_s as a result of the solid-phase resistance. Again voltage reduces as a result of the equilibrium potential at the -ve current collector V_{U-n}. Each and every voltage is described briefly.

3.3.1 Equilibrium Potential

This potential of an electrode in an ideal battery is described by the following equation named as Nernst equation:

$$V_{U-p} = U_o + \frac{RT}{nF} \ln\left(\frac{x_{\beta-i}}{x_{\alpha-i}}\right) + \frac{RT}{nF} \ln\left(\frac{\gamma_{\beta-i}}{x_{\gamma-i}}\right) \tag{3.1}$$

here i indicates the respective electrode (negative by n and positive is shown by p), also reference potential with U_o, universal gas constant with R, electrode temperature with T, number of electrons transferred in the reaction($n = 1$ for Li-ion) with n, Faradays constant with F , mole fraction with x and also α the Li-intercalated host material, β unoccupied host material and γ activity coefficient.

During discharging, Li-ions leave -ve electrode and travel towards the +ve electrode, as a result $x_{\alpha-n}$ and $x_{\beta-p}$ reduces, where as, $x_{\beta-n}$ and $x_{\alpha-p}$ increases. So, $V_{U-p} - V_{U-n}$ will decrease. The activity coefficient terms are unity in an ideal condition that is why the last term vanishes, bringing the actual structure of Nernst equation.

For the case of considered Li-ion battery, $x_{\beta-i} = 1 - x_{\alpha-i}$, so equation can be reconstructed by making this substitution. Then x_i is defined as $x_{\alpha-i}$ and dropping the α subscript:

$$V_{U-i} = U_o + \frac{RT}{nF} \ln\left(\frac{1 - x_i}{x_i}\right) + V_{INT,i} \tag{3.2}$$

whereas,

$$x_i = \frac{q_i}{q_{max}} \tag{3.3}$$

here amount of Li-ions is represented by q_i in electrode i, measured in Coulombs and q_i varies in the same direction as x_i.

where $q_{max} = q_p + q_n$ denotes the total available (i.e.mobile) Li-ions. So $x_p + x_n = 1$, Just after being charged fully, $x_p = 0.4$ and $x_n = 0.6$. Also, after full discharge, $x_p = 1$ and $x_n = 0$.

The activity correction term is $V_{INT,i}$ (which is 0 in the ideal condition). Since batteries constitutes non-ideal behaviour, hence the supposition of unity activity coefficients can not be applied. Terms like these are associated to surplus Gibbs free energy and can be expressed with the help of Redlich-Kister expansion:

$$V_{INT,i} = \frac{1}{nF}\left(\sum_{k=0}^{N_i} A_{i,k}\left((2x_i - 1)^{k+1} - \frac{2x_i k(1-x_i)}{(2x_i-1)^{1-k}}\right)\right) \tag{3.4}$$

Mentioned in the above expansion, the number of N_i terms and also the fitting parameters A_{i-k} are given in the Table 3.1.

TABLE 3.1: Battery Model Parameters [43]

Parameter	Value	Units
U_{op}	4.03	V
A_{p-0}	-33642.23	J/mol
A_{p-1}	0.11	//
A_{p-2}	23506.89	//
A_{p-3}	-74679.26	//
A_{p-4}	14359.34	//
A_{p-5}	307849.79	//
A_{p-6}	85053.13	//
A_{p-7}	-1075148.06	//
A_{p-8}	2173.62	//
A_{p-9}	991586.68	//
A_{p-10}	283423.47	//
A_{p-11}	-163020.34	//
A_{p-12}	-470297.35	//
U_{op}	0.01	V
A_{n-0}	86.19	J/mol

3.3.2 Concentration Overpotential

During the procedure of discharging, the reactions happening at the electrode surface results in the formation of concentration gradient. This is represented in Fig. 3.4. The concentration is almost even in the bulk volume, but near to the electrode the concentration varies abruptly. To handle with this situation, the total volume can be separated between the two control volumes, first is the bulk (b subscript) and second is the surface (s subscript).

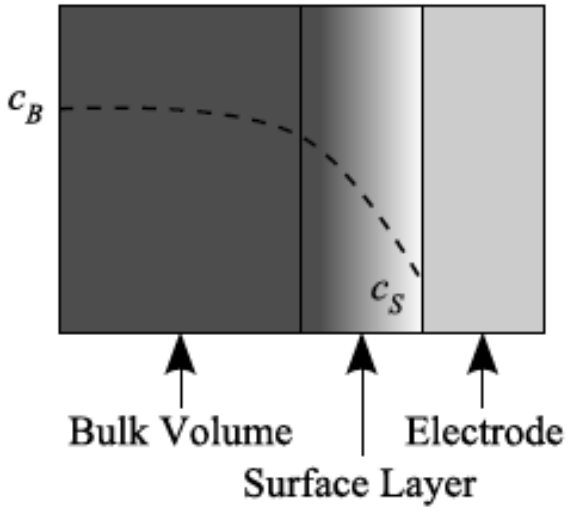

FIGURE 3.4: Concentration Gradient

For the two volumes, the derivation of the concentration is,

$$c_{b-i} = \frac{q_{b-i}}{v_{b-i}} \tag{3.5}$$

$$c_{s-i} = \frac{q_{s-i}}{v_{s-i}} \tag{3.6}$$

In the i^{th} electrode, v_{v-i} represents volume and c_{v-i} represents concentration of Li-ions. Similarly, $v_i = v_{b-i} + v_{s-i}$. Below mentioned relations gives:

$$q_p = q_{s-p} + q_{b-p} \tag{3.7}$$

$$q_n = q_{s-n} + q_{b-n} \tag{3.8}$$

$$q^{max} = q_{b-n} + q_{s-p} + q_{b-p} + q_{s-n} \tag{3.9}$$

During discharge process of a battery, Li-ions at the -ve electrode should disappear from its surface layer, via bulk, and start moving into the surface layer of the +ve electrode, making it comparable with the flow of electrons. The ions travel towards surface from the bulk layer by cause of concentration gradient. So, diffusion rate from bulk to surface layer can be explained as:

$$\dot{q}_{bs-i} = \frac{1}{D}(c_{b-i} - c_{s-i}) \tag{3.10}$$

here diffusion constant is represented by D.

The variables q(charge) are represented by:

$$\dot{q}_{s-p} = i_{App} + \dot{q}_{bs-p} \tag{3.11}$$

$$\dot{q}_{b-p} = -\dot{q}_{bs-p} + i_{App} - i_{App} \tag{3.12}$$

$$\dot{q}_{b-n} = -\dot{q}_{bs-n} + i_{App} - i_{App} \tag{3.13}$$

$$\dot{q}_{s-n} = -i_{App} + \dot{q}_{bs-n} \tag{3.14}$$

here applied electric current is defined by i_{App}. In the beginning, $c_{s-i} = c_{b-i}$, so diffusion is zero. As soon as discharge starts, ions start travelling from surface of the -ve electrode towards the bulk layer of -ve electrode, via separator to the bulk layer of the +ve electrode and finally on to the surface layer of the +ve electrode. When diffusion rate becomes less than the applied current, a gradient will be created within the surface and bulk volumes. When discharging ends, later the process of diffusion is active, also the equalization of concentrations takes place, resulting the increase in voltage (as concentration reduces on the surface layer of the +ve electrode, increasing voltage, and concentration in the surface layer of the -ve electrode becomes high, results in the increment of voltage).

Contrast in voltage of two CVs because of the dissimilarity in the concentration is defined as the concentration overpotential. Keeping in mind the definition of equilibrium potential, the potential at the bulk volume and at the surface; the contrast within them is the concentration overpotential. The expression for equilibrium potential at the layer of surface is:

$$V_{U-i} = U_o + \frac{RT}{nF} \ln \left(\frac{1 - x_{s-i}}{x_{s-i}} \right) + V_{INT,i} \tag{3.15}$$

where x_{s-i} is calculated by using

$$x_{s-i} = \frac{q_{s-i}}{q_{s-i}^{max}} \tag{3.16}$$

In the surface layer the mole fraction changes quickly as compared to mole fraction of bulk layer, giving the higher concentration gradient for smaller diffusion rates and larger applied current. The computed voltage relies on the procedure that is going on in the surface, not at bulk layer. As soon as the process of discharging ends, the surface becomes similar like bulk layer, responsible for restoration in the voltage. Thus the battery can be discharged more because surface layers are now reloaded with Li-ions in the -ve electrode.

3.3.3 Ohmic Overpotential

Solid-phase ohmic resistances are the cause of decrease in voltage, the electrolyte ohmic resistance, also current collectors resistances are considered as constant resistances and merged as:

$$V_o = V_{s-p} + V_{s-n} + V_e + V_{cc-p} + V_{cc-n} \tag{3.17}$$

$$V_o = i_{App}(R_{s-p} + R_{s-n} + R_e + R_{cc-p} + R_{cc-n}) \tag{3.18}$$

$$V_o = i_{App}R_o \tag{3.19}$$

where voltage drop at the current collectors is denoted as V_{cc}, also the current collector resistance for the electrode i is represented by R_{cc-i}.

3.3.4 Surface Overpotential

Because of SEI kinetics and charge transfer resistance, the overpotentials are represented by the Butler-Volmer equation. Here current is linear with the overpotential, for small current and that is directly proportional to log of the current for larger currents, also in the Butler-Volmer equation these two characteristics are merged:

$$J_i = J_{io}\left(exp\left(\frac{(1-\alpha)F}{RT}V_{\eta-i}\right) - exp\left(-\frac{\alpha F}{RT}V_{\eta-i}\right)\right) \tag{3.20}$$

where symmetry factor is denoted by α, J_i current density, and J_{io} is the exchange current density and these are defined as:

$$J_i = \frac{i}{S_i} \tag{3.21}$$

$$J_{io} = k_i(1 - x_{s-i})^{\alpha}(x_{s-i})^{(1-\alpha)} \tag{3.22}$$

where k_i is a parameter that is the combination of several constants including the electrolyte concentration a rate coefficient, and the maximum ion concentration. Reduction in voltage happens on the surface of electrode, hence for the execution of the exchange current density x_{s-i} is used.

The symmetry factor is 0.5 in the case of Li-ions, hence the equation of Butler-Volmer is made uncomplicated and rephrase in the form of voltage equation:

$$V_{\eta-i} = \frac{RT}{F\alpha} \operatorname{arcsinh}\left(\frac{J_i}{2J_{io}}\right) \tag{3.23}$$

3.3.5 State of Charge

Just after the LIB is fully charged, the SOC of a battery is normally expressed to be 1 and it is 0 as the battery becomes completely discharged. So in the battery model, it becomes similar to the mole fraction x_n, but extended from 0 to 1. Nominal SOC and apparent SOC are different terms. On the combination of the bulk and surface layer CVs in the negative electrode, nominal SOC is executed, while apparent SOC is determined relying on the surface layer. This will be defined as, the LIB can be discharged on a specific given rate, and also reach the voltage cutoff, i.e., apparent SOC becomes 0. On the other hand, as soon as the concentration gradient evens out, layer of surface is half filled and the Li-ion battery can be discharged more, i.e, nominal SOC remains the same while apparent SOC increases.
Nominal (n) and the apparent (a) SOC can be computed using:

$$SOC_n = \frac{q_n}{0.6q^{max}} \tag{3.24}$$

$$SOC_a = \frac{q_{s,n}}{0.6q^{max_{s,n}}} \tag{3.25}$$

here $q^{max_{s,n}} = q^{max}\frac{v_{s-n}}{v_n}$. Since the mole fraction at the positive electrode cannot decrease below 0.4 that is why the factor 1/0.6 is calculated, so SOC of 1 denotes the point where $q_n = 0.6q_{max}$.

3.3.6 Battery Terminal Voltage

Since every term related to voltage reduction in Fig. 3.3 has already been defined, the overall battery terminal voltage is computed as follows.

$$V_t = V_{U-p} - V_{U-n} - V_o - V_{\eta-p} - V_{\eta-n} \tag{3.26}$$

Internal battery voltages are not changed suddenly, rather the voltage changes smoothly. When the process of discharge stops, i.e, the increase in the voltage occur steadily as soon as surface layers shift to the concentrations of bulk volumes, created by the diffusion. Also, there are transients related with the terms V_o and $V_{\eta-i}$. To consider this in a more simpler way, the terminal voltage can be defined using:

$$V_t = V_{U-p} - V_{U-n} - V'_o - V'_{\eta-p} - V'_{\eta-n} \tag{3.27}$$

where,

$$\dot{V'_o} = \left(V_o - V'_o\right)/\tau_o \tag{3.28}$$

$$\dot{V'}_{\eta-p} = \left(V_{\eta-p} - V'_{\eta-p}\right)/\tau_{\eta-p} \tag{3.29}$$

$$\dot{V'}_{\eta-n} = \left(V_{\eta-n} - V'_{\eta-n}\right)/\tau_{\eta-n} \tag{3.30}$$

here the empirical time constants are represented by τ parameters.

The model states are $q_{s-p}, q_{b-p}, q_{b-n}, q_{s-n}, V'_o, V'_{\eta-p}, and V_{\eta-n}$. The single output of the model is V_t.

3.4 Battery Model with Considered Faults

The entire battery model is summarized in this section. The parameters of model are shown in Table 3.2. Some of the parameters are presented by the battery chemistry and dimensions.

TABLE 3.2: Model Parameters of LIB [43]

Parameter	Value	Units
q^{max}	1.32 x 10^4	C
R	8.314	J/mol/K
F	96487	C/mol
n	1	-
D	7.0 x 10^6	mol s/C/m^3
τ_o	10	s
α	0.5	-
R_o	0.085	Ω
S_p	2 x 10^{-4}	m^2
k_p	2 x 10^4	A/m^2
v_{s-p}	2 x 10^{-6}	m^3
v_{b-p}	2 x 10^{-5}	m^3
$\tau_{\eta-p}$	90	s
$\tau_{\eta-n}$	90	s
S_n	2 x 10^{-4}	m^2
k_n	2 x 10^4	A/m^2
v_{s-n}	2 x 10^{-6}	m^3
v_{b-n}	2 x 10^{-5}	m^3

$$\dot{q}_{s-p} = i_{App} + \frac{1}{D}\left(\frac{q_{b-p}}{v_{b-p}}\right) - \frac{1}{D}\left(\frac{q_{s-p}}{v_{s-p}}\right)$$

$$\dot{q}_{b-p} = -\frac{1}{D}\left(\frac{q_{b-p}}{v_{b-p}}\right) + \frac{1}{D}\left(\frac{q_{s-p}}{v_{s-p}}\right) + i_{App} - i_{App}$$

$$\dot{q}_{b-n} = -\frac{1}{D}\left(\frac{q_{b-n}}{v_{b-n}}\right) + \frac{1}{D}\left(\frac{q_{s-n}}{v_{s-n}}\right) + i_{App} - i_{App}$$

$$\dot{q}_{s-n} = -i_{App} + \frac{1}{D}\left(\frac{q_{b-n}}{v_{b-n}}\right) - \frac{1}{D}\left(\frac{q_{s-n}}{v_{s-n}}\right)$$

$$q^{max} = q_{s-p} + q_{b-p} + q_{s-n} + q_{b-n} + f_{q^{max}}$$

$$V_{U-i} = U_o + \frac{RT}{nF} \ln\left(\frac{1 - x_{s-i}}{x_{s-i}}\right) + V_{INT,i}$$

$$V_{INT,i} = \frac{1}{nF}\left(\sum_{k=0}^{N_i} A_{i-k}\left((2x_i - 1)^{k+1} - \frac{2x_i k(1 - x_i)}{(2x_i - 1)^{1-k}}\right)\right)$$

$$V_o = i_{App} R_o + f_{R_o}$$

$$V_{\eta-i} = \frac{RT}{F\alpha} \operatorname{arcsinh}\left(\frac{J_i}{2J_{io}}\right)$$

$$\dot{V}'_o = \left(V_o - V'_o\right)/\tau_o$$

$$\dot{V}'_{\eta-p} = \left(V_{\eta-p} - V'_{\eta-p}\right)/\tau_{\eta-p}$$

$$\dot{V}'_{\eta-n} = \left(V_{\eta-n} - V'_{\eta-n}\right)/\tau_{\eta-n}$$

$$V_t = V_{U-p} - V_{U-n} - V'_o - V'_{\eta-p} - V'_{\eta-n}$$

$$Y_{V_t} = V_t + f_{V_t}$$

$$Y_i = I + f_i$$

3.5 Aging of the Lithium-ion Battery

As described in chapter 2, aging of the battery can be demonstrated in two major ways [43]:

- First is the decrease in the capacity because of the parasitic and side reactions which are the cause of reduction of active (mobile) Li ions.
- Second is the increase in internal resistance because of the growth of SEI layer and other factors.

The capacity is normally calculated in regard to reference current and the related EOD as determined by cutoff voltage. In the Fig. 3.5 it has been mentioned clearly that if the capacity is decreased, that will make the voltage hitting the cut-off earlier and if the resistance increases that phenomenon would lower the overall

voltage, that also causes the voltage hitting the cutoff earlier. So both these aging processes cause loss of measured capacity.

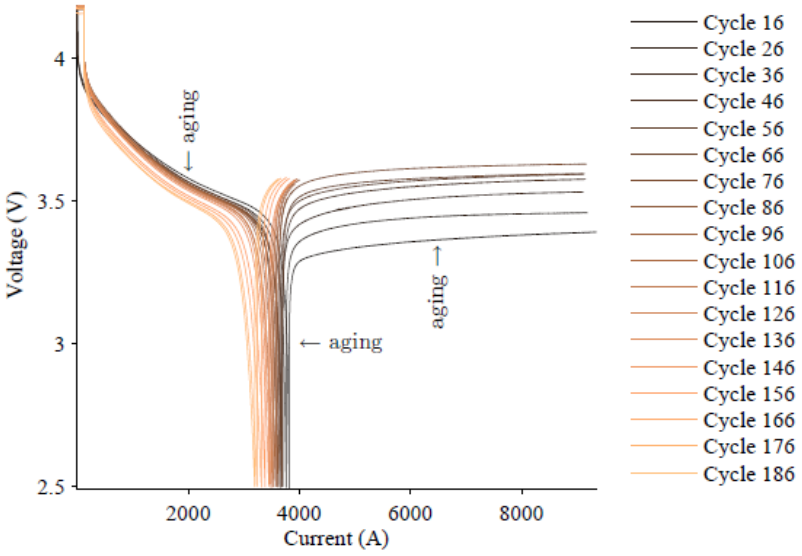

FIGURE 3.5: Battery Aging with 2A Discharge Curves [43].

3.5.1 Decrease in q^{max}

Inside the LIB model, q^{max} indicates the entire available charge inside the battery. Thus, the dissipation of active material (Li) can be demonstrated in the model by a change in q^{max}. The curve of discharge varies as q^{max} is decreased by 1% with each new discharge.

Figure. 3.6 represents the change in the discharge curve. A slight reduction in the voltage can be sensed, because of the Butler-Volmer term, that is relying on mole fraction which is calculated with the help of q^{max}. Also, EOD point reached earlier due to the discharge point being arrived with the less charge extracted. After discharge the Steady-state voltage increases as the cutoff is attained with less relative charge extracted.

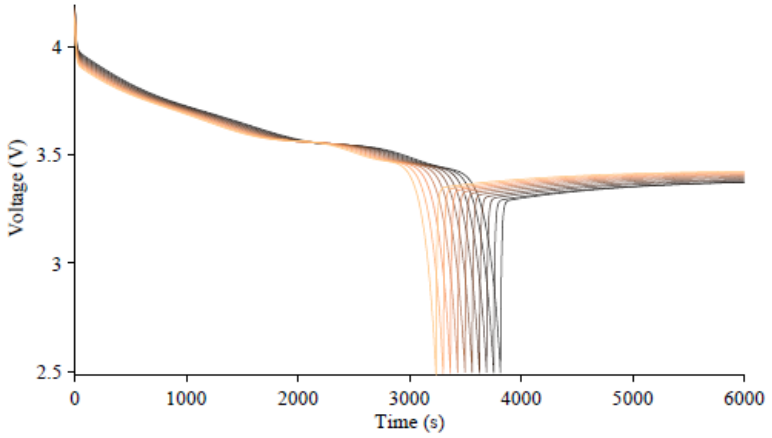

FIGURE 3.6: Decrease in q^{max} [43]

3.5.2 Increase in R_o

An increase in the R_o parameter is the root cause of increase in internal resistance. The change in the discharge curve, as R_o is increased by 5% with every new discharge is observed clearly in the Fig. 3.7.

The reduction in the voltage curve can be seen, but the change in EOD is not obvious, as the equilibrium potential contribution with some part from the Butler-Volmer dynamics dominates the dynamics near EOD. The variation in extracted charge is also not obvious therefore variations in steady-state voltage after discharge process becomes very less.

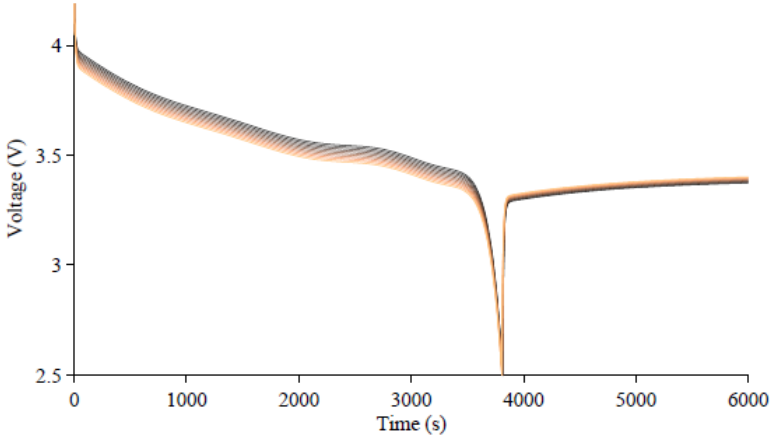

FIGURE 3.7: Increase in R_o [43]

3.5.3 Combined Effect of Decreasing q^{max} and Increasing R_o on Discharge Curve

The combined effects of q^{max} reducing with the amount of 1% and R_o extended by 5% with every new process of discharge, is represented in Fig. 3.8.

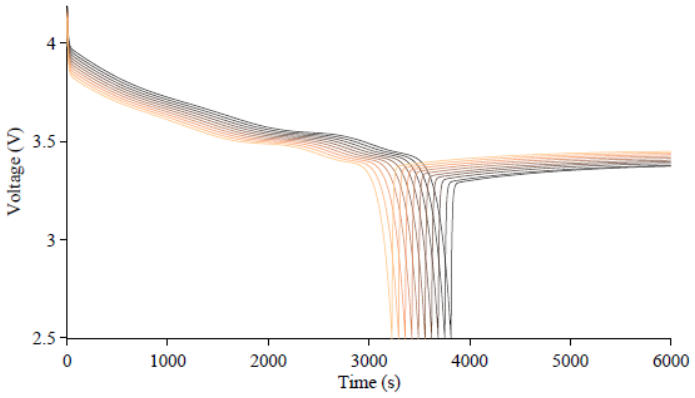

FIGURE 3.8: Decrease in q^{max} and Increase in R_o [43]

The change can be clearly seen in the discharge curve because of the reduction in q^{max}, but increase in R_o does not have any prominent effect, since the dynamics close to the EOD are influenced mostly with the equilibrium potential contribution with some of the part from Butler-Volmer properties.

3.6 Structural Analysis Based Fault Detection and Isolation Scheme

Structure analysis (SA) is a model-based scheme, that is mostly relies on the mathematical model of the system. The nobility of SA is to perform a fast and efficient analysis of fault detectability (FD) and fault isolability (FI) considering the possible faults in the battery system, perceive a degree of FD and FI by running the sensor placement method, and acquire a practical design of the methodology of FDI system. the main steps when applied in SA are shown in the Figure 3.9.

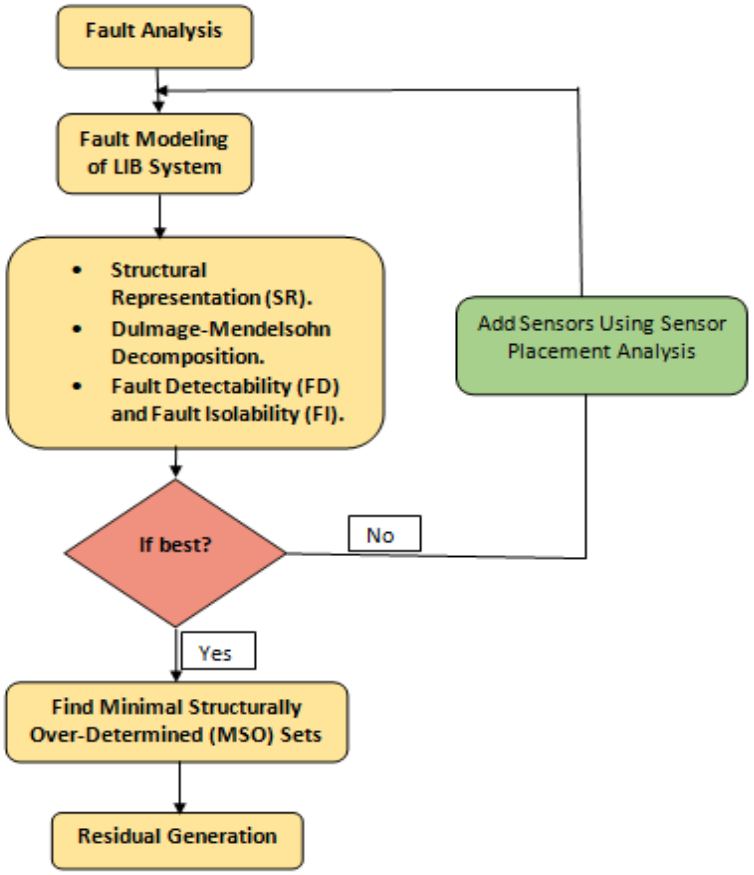

FIGURE 3.9: Main Steps involved in Structural Analysis

3.6.1 Fault Analysis for LIB

With the passage of time, technology is getting advanced, also Li-ion Batteries are gaining attention because of the benefits of high energy, low self discharge and high power density. These batteries are used in many applications such as in EVs passenger aircrafts and unmanned aerial vehicles. So battery sensors and internal fault detection and isolation is important to maintain the best battery performance while considering the aging factors also.

3.6.2 Structural Representation

Structural Analysis represents the basic properties and features of a system, and it is not dependent on model parameters. The structure of the LIB model represented by a bipartite graph with variables and equations as node sets [35, 36]. i.e.

which equation contains which variable. SA is represented in the form of incidence matrix in which the model equation connects with its respective known variables, unknown variables and faults. Therefore, In the model Structure,

System equations= $\{e_1, e_2, ...e_n\}$

Unknown variables= $\{x_1, x_2, ...x_n\}$

Known variables= $\{z_1, z_2, ...z_n\}$

Faults= $\{f_1, f_2, ...f_n\}$

whereas, n is the total number of equations, unknown variables, known variables or faults in the system.
A rough Structural representation of a system is shown in the Figure. 3.10

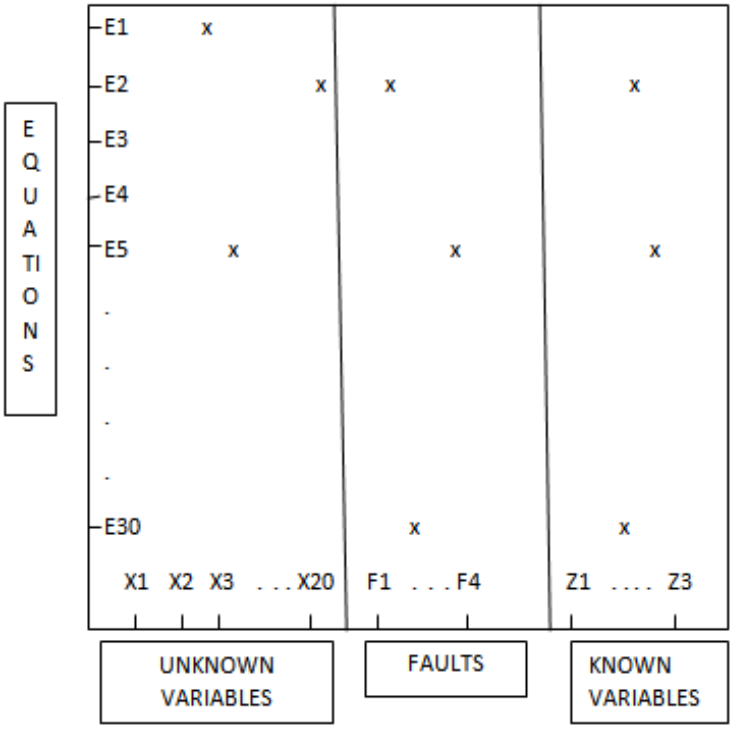

FIGURE 3.10: Basic Model Structure Representation

3.6.3 Dulmage-Mendelsohn Decomposition

DM decomposition represents a division (M_o, M_1.. M_n, M_∞) of the equation set M, same as the division of the unknown variables set(xs), and a partial order on sets M_i. If the columns and rows are repositioned according to this order, the bi-adjacency matrix has the upper block triangular form [44]. Three principle parts of M are; M^- is called the structurally under-determined part where the number of variables is less than that of equations. M^o the structurally just-determined part where the number of variables is equal to that of equations, and M^+ is the Structurally Over-determined (SO) part where the number of variables is greater than that of equations. The equation in which a fault f appears lies in the structurally (M^+) over-determined part. i.e $e_f \in M^+$, then fault f will be structurally detectable (SD).

According to the theory of SA, if the fault lies in M^o or M^- the fault is undetectable because no redundant equation has been found there. If the fault lies in M^+, the fault will be detectable as there is an additional (extra) equation which can generate a redundant relation.

The set, if M has more equations than unknowns variables is called Structurally Over-determined (SO) set.

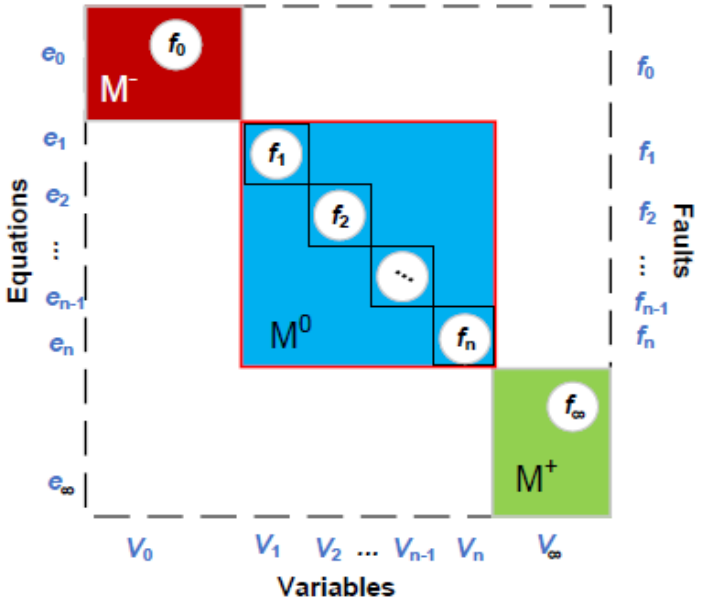

FIGURE 3.11: Schematic diagram of DM Decomposition

3.6.4 Fault Isolability Analysis

From Fault Isolability (FI) it means that if a fault can be differentiated from the other faults when that specific fault happens. If a fault f_i is isolable from f_j, this means that in the absence of equation e_{fj}, the equation e_{fi} still lie in SO part [45, 46] and can be represented as:

$$e_{fi} \in (M/e_{fj})^{+} \tag{3.31}$$

where e_{fi} and e_{fj} shows the equations containing faults f_i and f_j, M denotes the system Model and $(M/e_{fj})^{+}$ denotes that if equation e_{fj} is eliminated, the model will still be Structuraly Over-determined i.e the isolable fault e_{fi} is only associated to itself in the 2-D auto correlation matrix which is explained as Fault Isolation Matrix (FIM).

A rough sketch of FIM is shown in Figure. 3.12

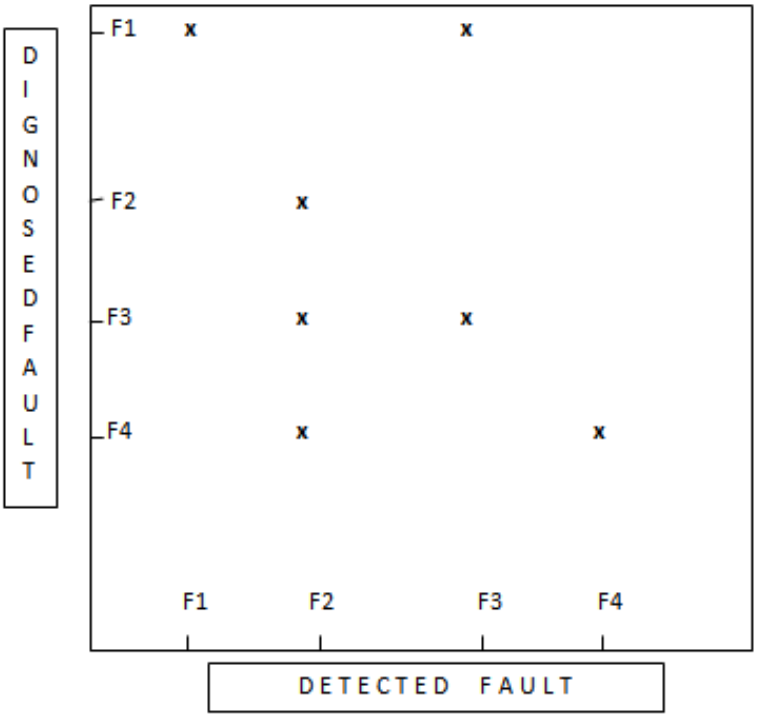

FIGURE 3.12: Schematic of FIM

3.6.5 Analysis of Sensor Placement Technique

Possible sensor selection, is the function of selecting a set of sensors so that maximum diagnosis specications are achieved [37]. This part will represent the benefits of important of sensor locations that will affect the performance of the proposed FDI scheme. Fault Detectability (FD) means that whether a fault in the system can be identified. Structural analysis (SA) is an efficient scheme for concluding that if the system faults are detectable and isolable for a given system or not.

An algorithm adopted from [37] is followed for analyzing which sensors should be added to meet a maximum diagnosis requirement specification related to fault detectability and fault isolability. The method is mostly based on the structural information in a model.

Initially in this method, possible sensor locations are specified first, which compute all minimal sensor sets. Then the sensor sets that achieve maximum fault isolability are preferred and executed.

3.6.6 Minimal Structurally Over-determined Sets

Finding MSO sets is an important step before residual design when SA is computed. In this work, an MSO-algorithm from [47] is deployed. The algorithm relies on a top-down approach in the sense that the entire model is started and then the size of the model is decreased step by step until a MSO set is left, while keeping the redundancy to produce a residual with the redundant equation. Redundancy can be defined as the system model has more equations than the unknown variables, The redundancy should be one in the end [48].

$$\phi(M^+) = |M^+| - |var_x(M^+)| = 1 \tag{3.32}$$

here $\phi(M)$ is the redundancy, M is the number of equations and var_x is the number of unknown variables.The redundancy part of the system model is also called structural over-determined part.

The purpose of using MSO sets is able to break down the complex system model into simple and small convenient sub- models, in which the diagnostic algorithm can be easily executed. Using algorithm we can find all possible MSO sets, from which the designers can choose the proper number of MSO sets, depending on the system diagnostic requirements.

Every MSO set is delicate to specific faults as the inputs u and sensor measurements y to ever MSO set is different, so faults in any of these sensors can be detected by using this MSO set. However, all faults can be efficiently isolated by using various MSO sets as different faults affect each MSO set differently. It is assumed that the concurrent appearance of different faults is ignored.

3.6.7 Residual Generation

In the literature, different approaches for residual generation, based on parity relations, EKF, adaptive/high gain/sliding-observers and many other, are found. But in SA two chief approaches are executed to generate residual generators that are automatic and supported by this scheme.

These two approaches are not the only solution, yet these are given preference because these approaches are convenient for automatic code generation [49]. The first is named as Sequential residual generation and second is a differential-algebraic observer technique suitable for the low-index problems in any system, and is called Observer based residual generator.

3.6.7.1 Sequential Residual Generation

In this scheme, given an overdetermined set of equations, a computational sequence for the unknown variables (x) is found, and then authenticate the consistency of the set of equations and observations by putting the variables into the residual equation [50].

In this method different dynamic systems are considered, hence to solve these differential constraints, there are two ways possible; either the equations are integrated or differentiated. In the end, the code found, can be so called derivative causality, integral causality, or mixed causality. In the mixed causality both the integral and differential causality are applied on the equations to generate residuals.

3.6.7.2 Observer Based Residual Generation

This method focus on generating code for an observer that estimates the unknown variables of the given system and executes a residual equation [51, 52].

The residual generator will be formulated as a DAE, which can be integrated using any standard ODE solver which means that it is applicable to low-index problems only [53, 54].

3.7 Electric Motor Model Example

For the better understanding of SA an example of electric model has been considered. The model has 9 equations and this model is relatively simpler than the battery model. All the steps of SA technique has been performed for the electric motor model.

3.7.1 Motor Model

$$
\begin{aligned}
V &= iR(1+f_R) + L\frac{di}{dt} + K_a iw \\
T_m &= K_a i^2 \\
J\frac{dw}{dt} &= T - bw \\
T &= T_m - T_I \\
\frac{d\theta}{dt} &= w \\
\frac{dw}{dt} &= \alpha \\
y_i &= i + f_i \\
y_w &= w + f_w \\
y_T &= T + f_T
\end{aligned}
$$

where V is voltage, i is current, T_m motor torque, T_I load torque, w rotational speed and θ motor angle.

3.7.2 Structural Representation

In this step structural model of the electric motor is shown in which each equation is connected with its respective unknown(x), known(z) and fault(f) variables. There are model equations on the y-axis of Figure 3.13, and on the x-axis respective unknown, known and fault variables are plotted.

3.7.3 DM Decomposition Plot of Electric Motor Model

In Figure 3.14 DM decomposition plot of electric motor model is shown. We can see that all model faults are detectable because all model faults are lying in the M^+ region.

The model is overdetermined because it has 9 equations, 4 unknown variables and 4 fault variables.

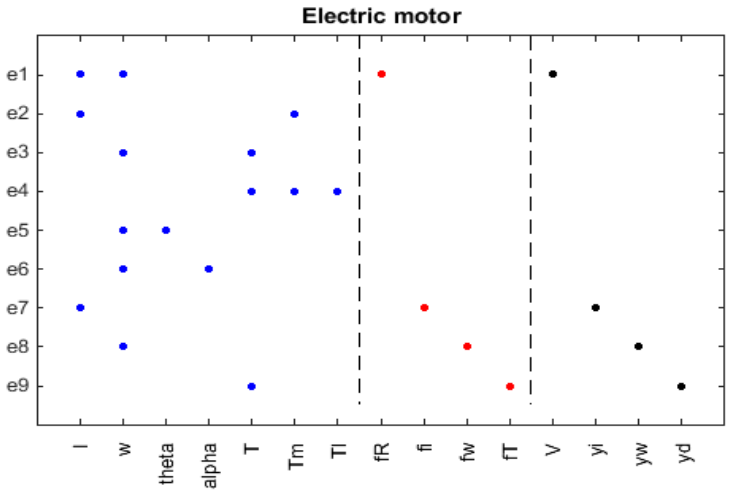

FIGURE 3.13: Electric motor model(Structural Representation)

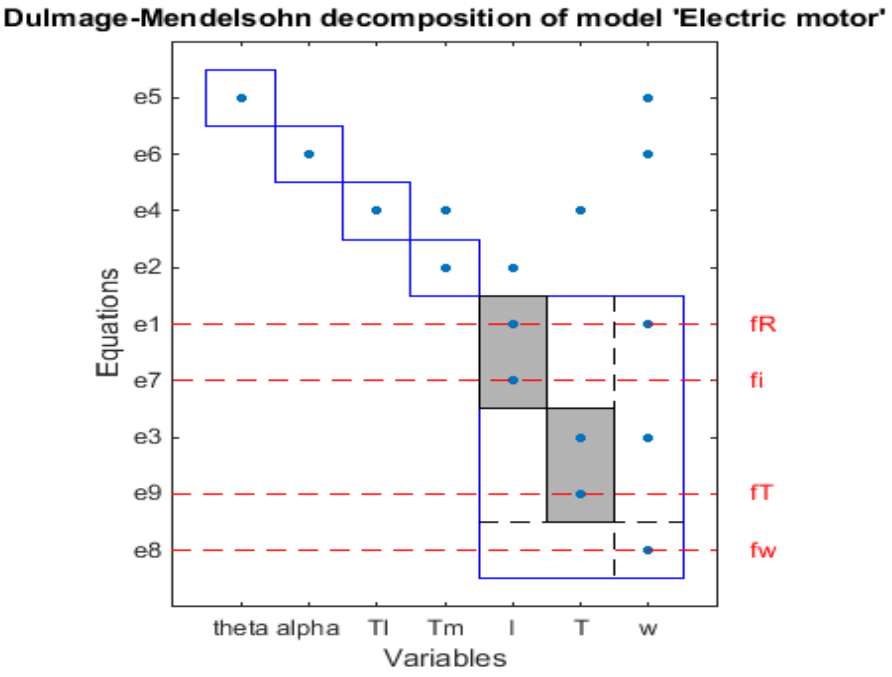

FIGURE 3.14: DM Decomposition Plot of Electric Motor

3.7.4 Fault Isolability Analysis of Electric Motor Model

In Figure 3.15 it is observed that the faults f_R and f_i are isolated from other two faults but cannot be isolated from each other.

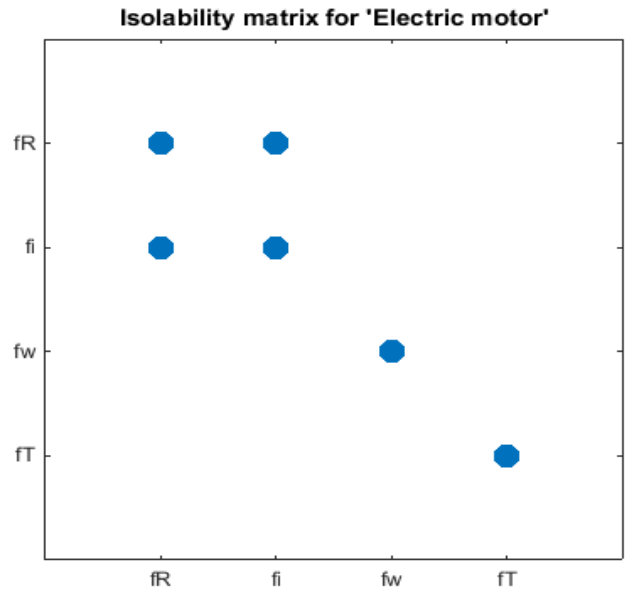

FIGURE 3.15: Isolability Matrix for Electric Motor Model

3.7.5 Sensor Placement Analysis

For the complete isolability of faults, sensor placement analysis has been performed. In this method locations of the required unknown variables were selected i.e i, T_m, T_i. In return we have got three different sensor sets, from which sensor set $S_1 = \{i\}$ was selected to achieve full isolability performance. After sensor

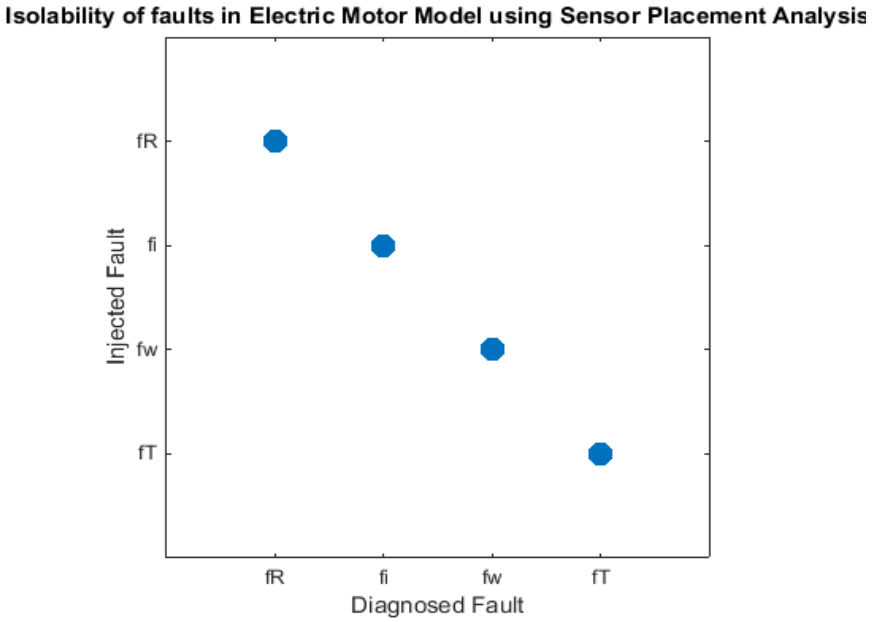

FIGURE 3.16: Isolability of the faults after sensor placement analysis

placement analysis method it is observed that all faults are uniquely isolable from each other.

3.7.6 MSO Sets

After sensor placement analysis, 6 MSO sets have been generated. Finding MSO sets is an important part before designing residuals. In Figure 3.17 steps for the

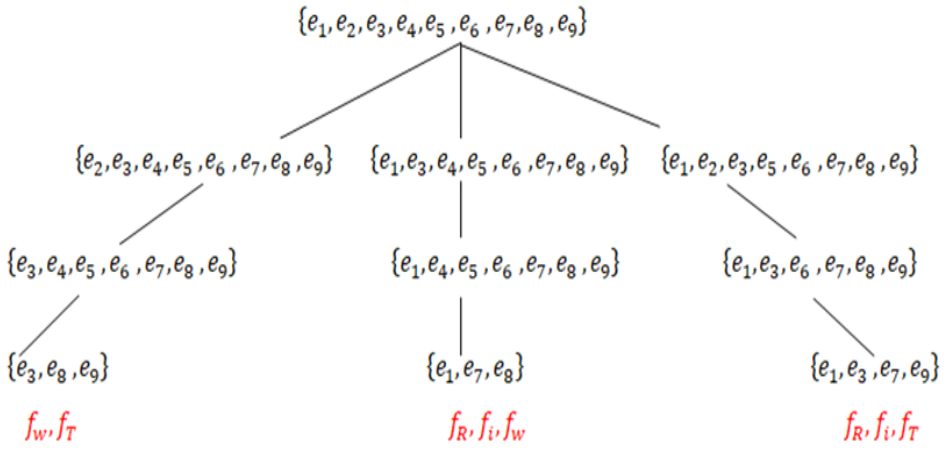

FIGURE 3.17: MSO generation steps

generation of MSO sets has been depicted clearly. Each MSO set is sensitive to different sets of faults.

3.7.7 Sequential Residual Generation

If MSO set $\{e_1, e_5, e_6\}$ is taken then residual can be generated as depicted in the following steps.

$$e1 : V - i(R + f_R) - L\frac{di}{dt} - K_a iw = 0$$

$$e5 : i = y_i - f_i$$

$$e6 : w = y_w - f_w$$

Residual Equation is:

$$\begin{aligned} r =& V - y_i R + L\frac{dy_i}{dt} - K_a y_i y_w \\ r =& y_i f_R + f_i(K_a f_w - R - y_w - f_R) - L\frac{df_i}{dt} - K_a y_i f_w \end{aligned}$$

e1 was selected as residual equation. Residual from $\{e_1, e_5, e_6\}$ is sensitive to the faults $\{f_i, f_w, f_R\}$. This is how sequential residual generation is performed. Unknowns are found sequentially, finally values of these unknowns are then inserted into a selected residual equation.

3.7.8 Observer Based Residual Generation for Motor

In this method, the values of unknowns are estimated using feedback observer. If MSO set $\{e_1, e_5, e_6\}$ is taken then residual can be generated as depicted in the following steps.

$$\begin{aligned} e6 : \hat{w} =& y_w \\ e1 : \frac{d\hat{i}}{dt} =& \frac{1}{L}(V - \hat{i}R - K_a\hat{i}\hat{w}) \\ e5 : r1 =& y_i - \hat{i} \end{aligned}$$

Chapter 4

Simulation and Results

4.1 LIB Structural Representation

In this section the basic properties and features of the LIB system are represented by Structural Analysis. The structure of the LIB model is shown by a bipartite graph with variables and equations as node sets. SA is represented in the form of incidence matrix in which the model equation connects with its respective known variables, unknown variables and faults and can be represented as:

System equations= $\{e_1, e_2, ...e_{30}\}$

Unknown Variables Set= $\left\{q_{s,p}, q_{s,n}, q_{b,p}, q_{b,n}, V_o, I, V_t, q_p, q_n, x_p, x_n, q_{s,p}^{max}, q_{s,n}^{max}, \right\}$

$\left\{J_p, J_n, J_{po}, J_{no}, x_{s,p}, x_{s,n}, V_{U,p}, V_{U,n}, V_{\eta,p}, V_{\eta,n}, V_o', V_{\eta,p}', V_{\eta,n}'\right\}$

Known variables Set= $\{q^{max}, y_i, y_{v_t}\}$

Faults Set= $\{f_{V_t}, f_I, f_{R_o}, f_{q^{max}}\}$

The Structural Representation of Li-ion Battery is shown in the Figure. 4.1 in which it has been shown that how each equation is connected with its unknown, known and faults variables respectively.

In the Li-ion battery model, as discussed in chapter 3, four faults are considered, in which two are voltage (f_{V_t}) and current (f_I) sensor faults and the remaining two are internal faults; increase in internal resistance (f_{R_o}) and decrease in total amount of available Li-ions ($f_{q^{max}}$).

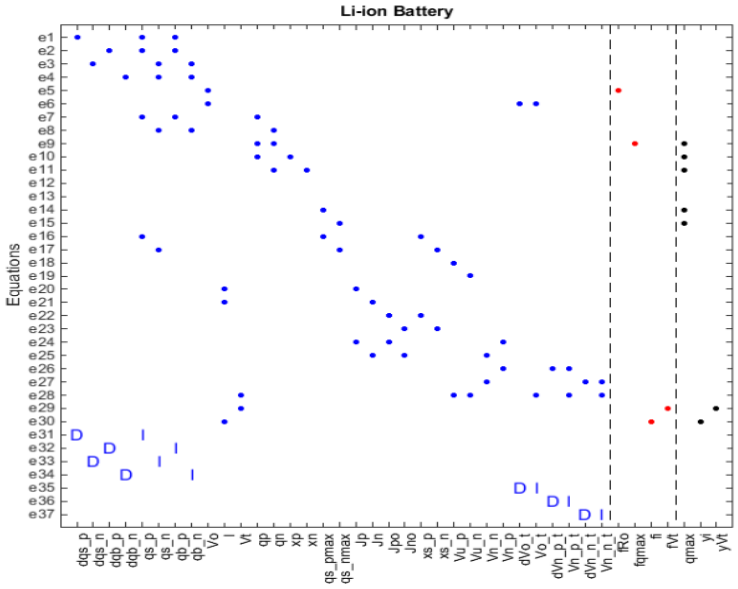

FIGURE 4.1: Structural Model of Li-ion Battery

4.2 DM Decomposition for LIB Model

Since the battery model is redundant because there are additional equations (30 equations) than unknown variables (26 unknown variables). The over-determined part of the model could be found by analyzing the unknown part of the structural model with DulmageMendelsohn (DM) decomposition which could arrange the rows and columns of the incidence matrix into an upper triangular form, and the

unknown part could be decomposed into three parts: M^-, M^o, M^+.

In the Figure below the blue rectangle shows M^+ i.e over-determined part of the LIB model. From the DM Decomposition plot it can be seen that all system faults are detectable, as these faults are located in structural over-determined part. Gray shaded rectangles show the equivalence classes. The faults appearing in the same equivalence are isolable from other system faults but can not be isolated from each other.

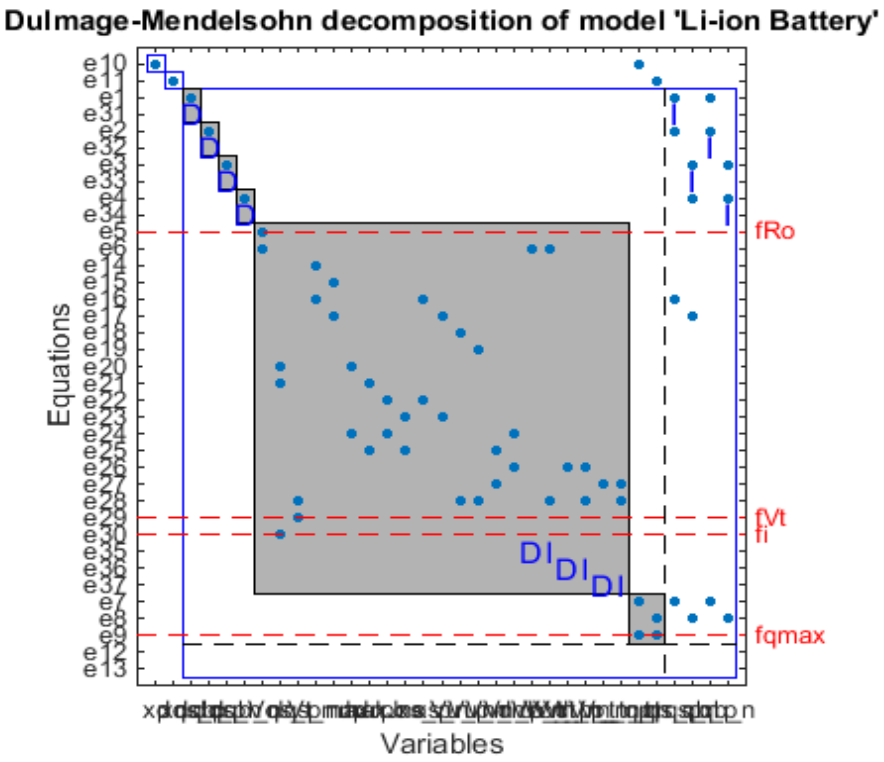

FIGURE 4.2: DM Decomposition of Structural Model of LIB

4.3 Diagnosability Analysis of LIB Model

To illustrate single fault isolability performance isolability matrix is computed. Analysis can be restricted to causality assumptions which here means that the analysis can be done in integral causality, derivative causality or mixed causality. Diagnosability means to analyze which faults that are structurally detectable and

structurally isolable.

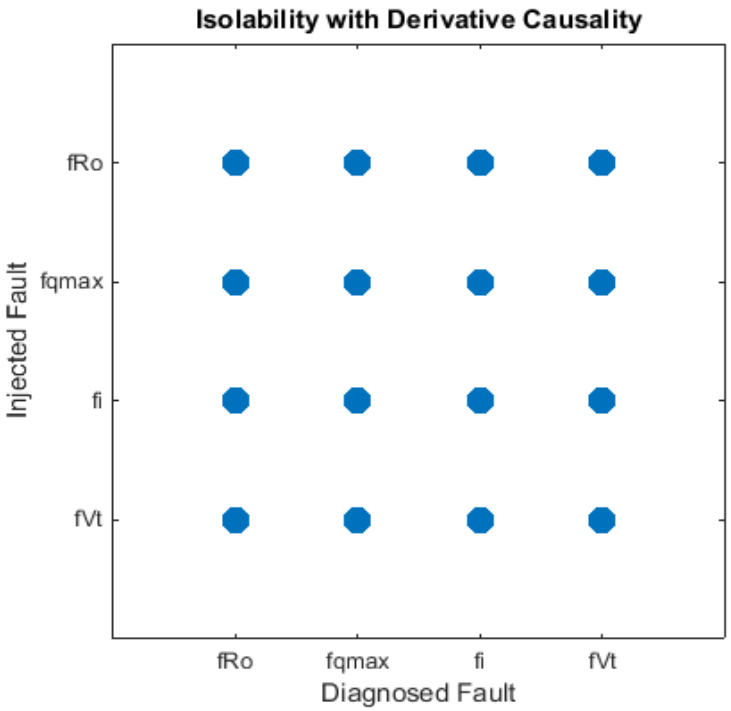

FIGURE 4.3: Isolability of LIB Faults using Derivative Causality

In the Figure.4.3 Derivative causality is applied to check the isolability of LIB faults.

The matrix of isolability shows how the fault isolability performance has been degraded, when the techniques of residual generation are limited to Derivative causality based methods. This Figure demonstrates that the isolability matrix, where a dot in position (i,j) indicates that, structurally, fault fi can not be isolated from fault fj.

In Figure.4.4 and Figure.4.5 fault isolability performance has been represented, when residual generation techniques are limited to integral and mixed causality based methods respectively. In both the cases faults are still not isolated.

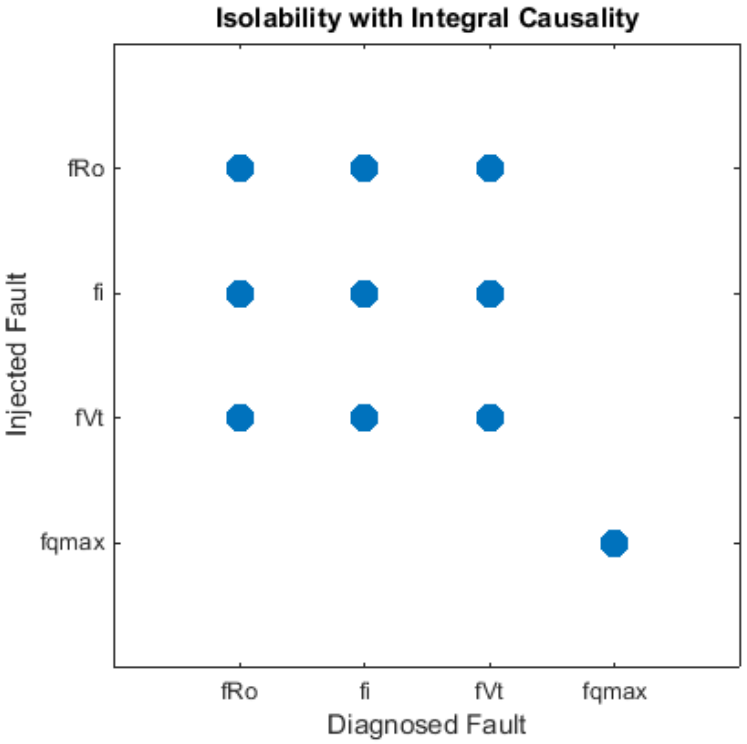

FIGURE 4.4: Isolability of LIB Faults using Integral Causality

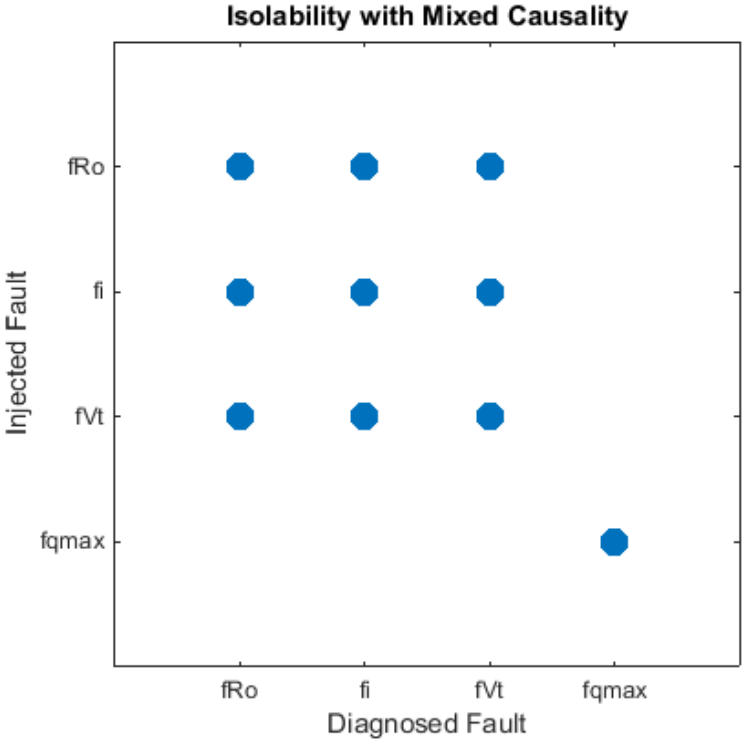

FIGURE 4.5: Isolability of LIB Faults using Mixed Causality

4.4 Sensor Placement Analysis for LIB

Since, it has been found out in the isolability section that three of the faults are not isolable from each other. So, here we will add some sensors to isolate these faults with the help of Sensor placement Analysis.

This technique has been used to increase the isolability performance of the LIB system faults. First, the possible sensor locations are specified then, a set of sensors will be selected such that maximum isolability of faults can be reached.

The possible sensor locations selected were, V_o, I, V_t. In return three minimal sensor sets were generated out which first sensor set $\{I, V_t\}$ has been selected according to Diagnosis requirements of LIB system.

It can be seen in Figure.4.6 that after adding desired sensors, all faults of LIB system were completely isolated.

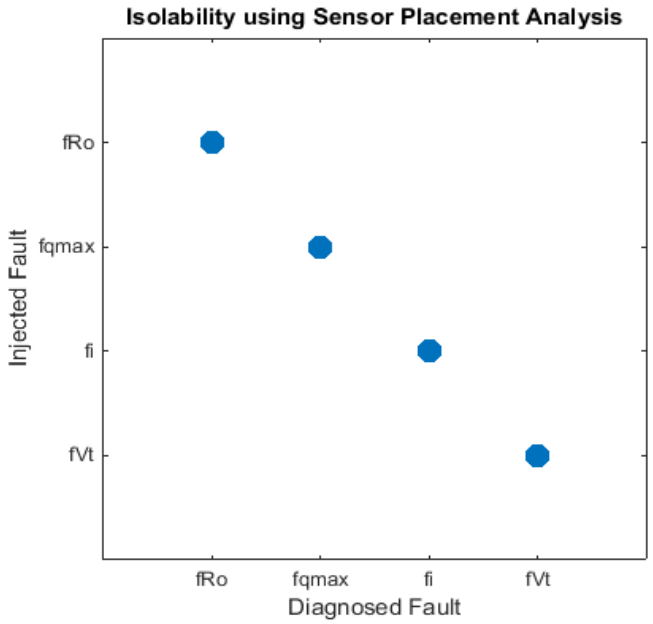

FIGURE 4.6: Isolability of faults after Sensor Placement Analysis

The sensors that are new may also prone to the faults. To check this, repeat the process of sensor placement analysis, which will produce Figure.4.7. Here a new

fault has generated in the analysis, this is the fault in the new sensor.

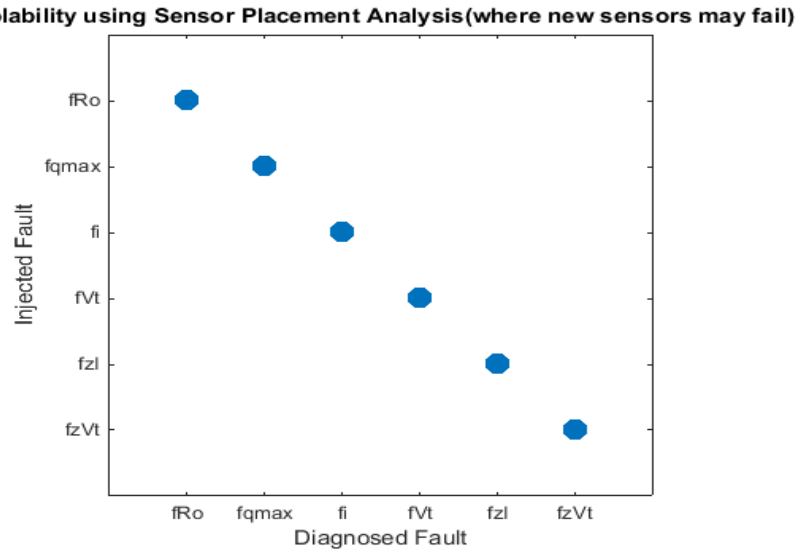

FIGURE 4.7: Isolability of faults after Sensor Placement Analysis (where new sensors may fail)

After adding sensors, the Fault isolability can also be validated through DM Decomposition plot. Figure.4.8 shows the results of fault isolability after sensor placement. It can be clearly seen that all faults have been isolated completely.

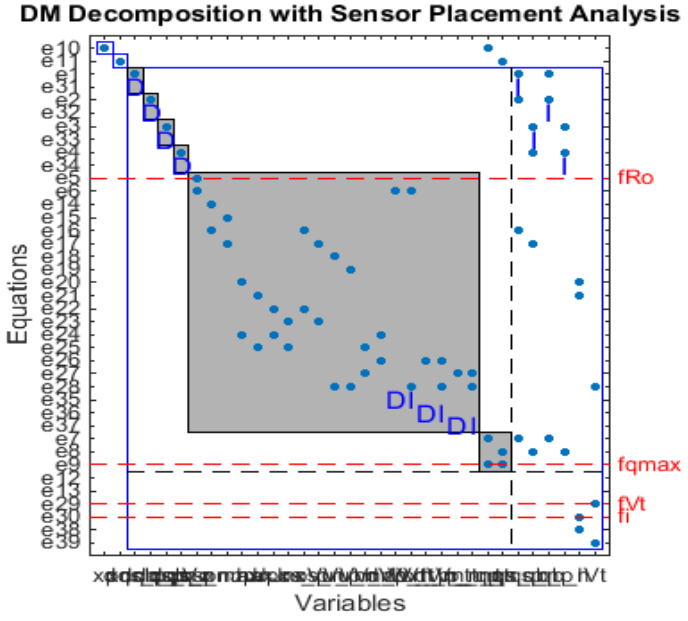

FIGURE 4.8: DM Decomposition of the LIB Model after Sensor placement analysis

4.5 MSO Sets Selection for LIB

MSO sets selection is an important step before the residual design when SA scheme is executed. In the structural analysis of LIB 25 MSO sets have been found, from which four best MSO sets were considered. The selected Minimal Testable sets are given in Table.4.1 corresponding to their equations. Each MSO set is sensitive to different system faults. Figure.4.9 contains the isolability matrix which has been

TABLE 4.1: Selected Minimal Testable Sets

MSO Sets	Contained Equations
$MSO21$	$\{e1-e4, e7-e9, e31-e34\}$
$MSO22$	$\{e1-e6, e14-e28, e31-e39\}$
$MSO23$	$\{e1-e6, e14-e28, e30-e37, 39\}$
$MSO24$	$\{e1-e6, e14-e29, e31-e38\}$

found using all 25 MSO sets. This matrix depicts that if we use all 25 MSO sets full isolability of faults can be achieved.

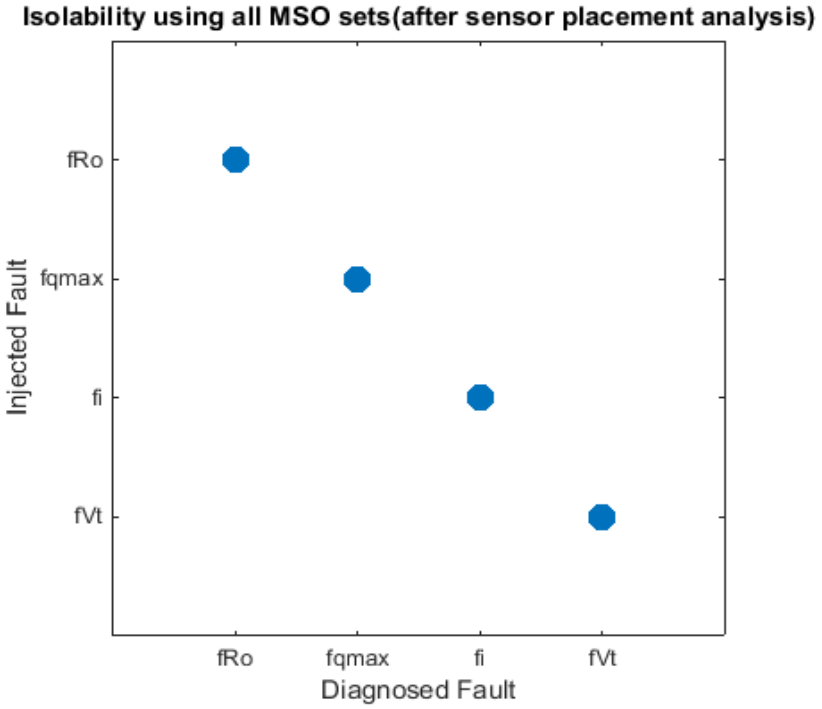

FIGURE 4.9: Isolability of LIB Faults using all MSO sets

4.6 Observer Based Residual Generation for LIB

According to above 4 MSO sets, four residuals can be generated accordingly.
In this case no residual equation is needed to be specified, the approach selects residual equations automatically. Observer based residual technique is only applied to low-index problems.

4.6.1 Residual 1

Residual-1 can be generated by using the MSO21, where 11 equations are involved. The equations are $\{e1 - e4, e7 - e9, e31 - e34\}$.

4.6.2 Residual 2

Residual-2 can be generated by using the MSO22, where 30 equations are involved. The equations are $\{e1 - e6, e14 - e28, e31 - e39\}$.

4.6.3 Residual 3

Residual-3 can be generated by using the MSO23, where 30 equations are involved. The equations are $\{e1 - e6, e14 - e28, e30 - e37, 39\}$

4.6.4 Residual 4

Residual-4 can be generated by using the MSO24, where 30 equations are involved. The equations are $\{e1 - e6, e14 - e29, e31 - e38\}$.

4.6.5 Fault Signature Matrix using 4 Residuals

In Figure.4.10, sensitivity of each residual to the modelled faults has been shown.

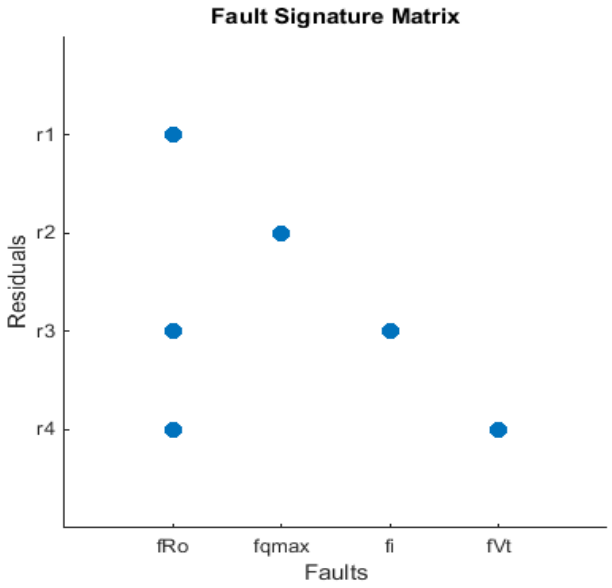

FIGURE 4.10: Detectability of the 4 residuals for LIB Model

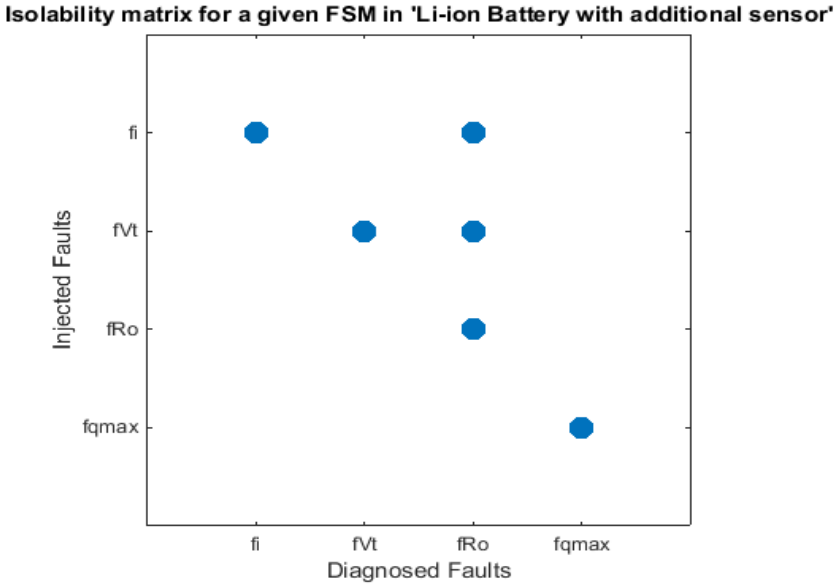

FIGURE 4.11: FSM of Faults using 4 residuals

In Figure.4.11, isolability of the faults corresponding to each residual has been shown.

Here only four MSO sets are used i.e $M21, M22, M23, M24$. If all 25 MSO sets were to be used full fault isolability would be achieved.

Next, in the Table.4.2 the symbol $\bullet$ indicates that fault can be detected by the residual and $\circ$ shows that fault is undetectable.

TABLE 4.2: Detectability of faults using 4 Residuals

Residuals	f_{R_o}	$f_{q^{max}}$	f_i	fV_t	*MSOSets*	*Equations*
$R1$	●	○	○	○	$MSO22$	$\{e1-e6, e14-e28, e31-e39\}$
$R2$	○	●	○	○	$MSO21$	$\{e1-e4, e7-e9, e31-e34\}$
$R3$	●	○	●	○	$MSO23$	$\{e1-e6, e14-e28, e30-e37, 39\}$
$R4$	●	○	○	●	$MSO24$	$\{e1-e6, e14-e29, e31-e38\}$

Chapter 5

Conclusion and Future Work

5.1 Conclusion

In this work a model-based FDI scheme for the Li-ion battery to detect and isolate the sensor and internal system faults is presented. The internal system faults are the major cause of aging in Li-ion batteries.

The scheme relies on the observer based residual generation using SA theory. The fault detectability and isolability can be achieved by SA, without having the accurate information of battery parameters. To achieve maximum fault isolability sensor placement analysis is used. This scheme is very useful for faster identification of the analytical redundancy part, i.e structural over-determined part, by investigating the structural model represented by an incidence matrix. With the help of selected minimal structurally over-determined (MSO)sets, different diagnostic tests can be constructed. Then these sets are further used to generate residuals for FD and FI purpose.
The simulations results confirmed that fq^{max}, fR_o, fi and fV_t can be uniquely isolated.

5.2 Future Work

The work that has been carried out in the thesis can be extended in many other ways. In the future, an experimental platform can be performed to authenticate the performance of the presented FDI system. Also, to evaluate extracted residual generators with measured real data, in order to explore sensitivity to faults in the presence of measurement noise, disturbance and modeling errors.

Bibliography

[1] K. Mizushima, P. Jones, P. Wiseman, and J. B. Goodenough, "A new cathode material for batteries of high energy density," *Materials Research Bulletin*, vol. 15, no. 6, pp. 783–789, 1980.

[2] N. Omar, M. Al Sakka, M. Daowd, O. Coosemans, P. Van den Bossche, and J. Van Mierlo, "Development of a thermal model for lithium-ion batteries for plug-in hybrid electric vehicles," *World Electric Vehicle Journal*, vol. 5, no. 2, pp. 300–306, 2012.

[3] N. Omar, P. Van den Bossche, G. Mulder, M. Daowd, J. Timmermans, J. Van Mierlo, and S. Pauwels, "Assessment of performance of lithium iron phosphate oxide, nickel manganese cobalt oxide and nickel cobalt aluminum oxide based cells for using in plug-in battery electric vehicle applications," in *2011 IEEE Vehicle Power and Propulsion Conference*. IEEE, 2011, pp. 1–7.

[4] D. Deng, M. G. Kim, J. Y. Lee, and J. Cho, "Green energy storage materials: Nanostructured and sn-based anodes for lithium-ion batteries," *Energy & Environmental Science*, vol. 2, no. 8, pp. 818–837, 2009.

[5] A. Yoshino, "The birth of the lithium-ion battery," *Angewandte Chemie International Edition*, vol. 51, no. 24, pp. 5798–5800, 2012.

[6] A. Du Pasquier, I. Plitz, S. Menocal, and G. Amatucci, "A comparative study of li-ion battery, supercapacitor and nonaqueous asymmetric hybrid devices for automotive applications," *Journal of power sources*, vol. 115, no. 1, pp. 171–178, 2003.

[7] J.-M. Tarascon and M. Armand, "Issues and challenges facing rechargeable lithium batteries," in *Materials for Sustainable Energy: A Collection of Peer-Reviewed Research and Review Articles from Nature Publishing Group*. World Scientific, 2011, pp. 171–179.

[8] H. Arai, S. Okada, Y. Sakurai, and J. Yamaki, "Thermal behavior of linio2 and the decomposition mechanism," *Solid State Ionics*, vol. 109, no. 3-4, pp. 295–302, 1998.

[9] Y. Gao, J. Jiang, C. Zhang, W. Zhang, Z. Ma, and Y. Jiang, "Lithium-ion battery aging mechanisms and life model under different charging stresses," *Journal of Power Sources*, vol. 356, pp. 103–114, 2017.

[10] E. Prada, D. Di Domenico, Y. Creff, J. Bernard, V. Sauvant-Moynot, and F. Huet, "A simplified electrochemical and thermal aging model of lithium iron phosphate graphite li-ion batteries: Power and capacity fade simulations," *Journal of The Electrochemical Society*, vol. 160, no. 4, pp. 616–628, 2013.

[11] N. Omar, Y. Firouz, H. Gualous, J. Salminen, T. Kallio, J. Timmermans, T. Coosemans, P. Van den Bossche, and J. Van Mierlo, "Aging and degradation of lithium-ion batteries," in *Rechargeable Lithium Batteries*. Elsevier, 2015, pp. 263–279.

[12] V. Ramadesigan, P. W. Northrop, S. De, S. Santhanagopalan, R. D. Braatz, and V. R. Subramanian, "Modeling and simulation of lithium-ion batteries from a systems engineering perspective," *Journal of the electrochemical society*, vol. 159, no. 3, pp. 31–45, 2012.

[13] B. Saha and K. Goebel, "Modeling li-ion battery capacity depletion in a particle filtering framework," in *Proceedings of the annual conference of the prognostics and health management society*, 2009, pp. 2909–2924.

[14] M. Daigle, A. Saxena, and K. Goebel, "An efficient deterministic approach to model-based prediction uncertainty estimation," Tech. Rep., 2012.

[15] K. Kumaresan, G. Sikha, and R. E. White, "Thermal model for a li-ion cell," *Journal of the Electrochemical Society*, vol. 155, no. 2, pp. 164–171, 2008.

[16] G. Ning and B. N. Popov, "Cycle life modeling of lithium-ion batteries," *Journal of The Electrochemical Society*, vol. 151, no. 10, pp. 1584–1591, 2004.

[17] M. Doyle, T. F. Fuller, and J. Newman, "Modeling of galvanostatic charge and discharge of the lithium/polymer/insertion cell," *Journal of the Electrochemical society*, vol. 140, no. 6, pp. 1526–1533, 1993.

[18] J. Newman and W. Tiedemann, "Porous-electrode theory with battery applications," *AIChE Journal*, vol. 21, no. 1, pp. 25–41, 1975.

[19] K.-J. Lee, K. Smith, A. Pesaran, and G.-H. Kim, "Three dimensional thermal-, electrical-, and electrochemical-coupled model for cylindrical wound large format lithium-ion batteries," *Journal of Power Sources*, vol. 241, pp. 20–32, 2013.

[20] M. B. Pinson and M. Z. Bazant, "Theory of sei formation in rechargeable batteries: capacity fade, accelerated aging and lifetime prediction," *Journal of the Electrochemical Society*, vol. 160, no. 2, pp. 243–250, 2013.

[21] A. Eddahech, O. Briat, R. Chaari, N. Bertrand, H. Henry, and J.-M. Vinassa, "Lithium-ion cell modeling from impedance spectroscopy for ev applications," in *2011 IEEE Energy Conversion Congress and Exposition*. IEEE, 2011, pp. 1449–1453.

[22] Y. Zhang, C.-Y. Wang, and X. Tang, "Cycling degradation of an automotive lithium iron phosphate lithium-ion battery," *Journal of Power Sources*, vol. 196, no. 3, pp. 1513–1520, 2011.

[23] C. R. Birkl, M. R. Roberts, E. McTurk, P. G. Bruce, and D. A. Howey, "Degradation diagnostics for lithium ion cells," *Journal of Power Sources*, vol. 341, pp. 373–386, 2017.

[24] S. S. Choi and H. S. Lim, "Factors that affect cycle-life and possible degradation mechanisms of a li-ion cell based on licoo2," *Journal of Power Sources*, vol. 111, no. 1, pp. 130–136, 2002.

[25] M. Kabir and D. E. Demirocak, "Degradation mechanisms in li-ion batteries: a state-of-the-art review," *International Journal of Energy Research*, vol. 41, no. 14, pp. 1963–1986, 2017.

[26] A. Eddahech, O. Briat, E. Woirgard, and J.-M. Vinassa, "Remaining useful life prediction of lithium batteries in calendar ageing for automotive applications," *Microelectronics Reliability*, vol. 52, no. 9-10, pp. 2438–2442, 2012.

[27] I. Bloom, B. Cole, J. Sohn, S. Jones, E. Polzin, V. Battaglia, G. Henriksen, C. Motloch, R. Richardson, T. Unkelhaeuser *et al.*, "An accelerated calendar and cycle life study of li-ion cells," *Journal of Power Sources*, vol. 101, no. 2, pp. 238–247, 2001.

[28] Q. Zhang and R. E. White, "Calendar life study of li-ion pouch cells: Part 2: Simulation," *Journal of Power Sources*, vol. 179, no. 2, pp. 785–792, 2008.

[29] M. Kassem, J. Bernard, R. Revel, S. Pelissier, F. Duclaud, and C. Delacourt, "Calendar aging of a graphite/lifepo4 cell," *Journal of Power Sources*, vol. 208, pp. 296–305, 2012.

[30] M. Blanke, M. Kinnaert, J. Lunze, M. Staroswiecki, and J. Schröder, *Diagnosis and fault-tolerant control*. Springer, 2006, vol. 2.

[31] W. Chen, W.-T. Chen, M. Saif, M.-F. Li, and H. Wu, "Simultaneous fault isolation and estimation of lithium-ion batteries via synthesized design of luenberger and learning observers," *IEEE Transactions on Control Systems Technology*, vol. 22, no. 1, pp. 290–298, 2013.

[32] J. Marcicki, S. Onori, and G. Rizzoni, "Nonlinear fault detection and isolation for a lithium-ion battery management system," in *ASME 2010 Dynamic Systems and Control Conference*. American Society of Mechanical Engineers, 2010, pp. 607–614.

[33] A. Sidhu, A. Izadian, and S. Anwar, "Adaptive nonlinear model-based fault diagnosis of li-ion batteries," *IEEE Transactions on Industrial Electronics*, vol. 62, no. 2, pp. 1002–1011, 2014.

[34] E. Balaban, A. Saxena, P. Bansal, K. F. Goebel, and S. Curran, "Modeling, detection, and disambiguation of sensor faults for aerospace applications," *IEEE Sensors Journal*, vol. 9, no. 12, pp. 1907–1917, 2009.

[35] M. A. Djeziri, B. O. Bouamama, G. Dauphin-Tanguy, and R. Merzouki, "Lft bond graph model-based robust fault detection and isolation," in *Bond graph modelling of engineering systems*. Springer, 2011, pp. 105–133.

[36] D. Düştegör, E. Frisk, V. Cocquempot, M. Krysander, and M. Staroswiecki, "Structural analysis of fault isolability in the damadics benchmark," *Control Engineering Practice*, vol. 14, no. 6, pp. 597–608, 2006.

[37] M. Krysander and E. Frisk, "Sensor placement for fault diagnosis," *IEEE Transactions on Systems, Man, and Cybernetics-Part A: Systems and Humans*, vol. 38, no. 6, pp. 1398–1410, 2008.

[38] Z. Liu, H. He, Q. Ahmed, and G. Rizzoni, "Structural analysis based fault detection and isolation applied for a lithium-ion battery pack," *IFAC-PapersOnLine*, vol. 48, no. 21, pp. 1465–1470, 2015.

[39] Q. Chen, Q. Ahmed, G. Rizzoni, and M. Qiu, "Design and evaluation of model-based health monitoring scheme for automated manual transmission," *Journal of Dynamic Systems, Measurement, and Control*, vol. 138, no. 10, p. 101011, 2016.

[40] R. Isermann, "Model-based fault-detection and diagnosis–status and applications," *Annual Reviews in control*, vol. 29, no. 1, pp. 71–85, 2005.

[41] Z. Liu, Q. Ahmed, G. Rizzoni, and H. He, "Fault detection and isolation for lithium-ion battery system using structural analysis and sequential

residual generation," in *ASME 2014 Dynamic Systems and Control Conference*. American Society of Mechanical Engineers, 2014, pp. V002T36A005–V002T36A005.

[42] Z. Liu, Q. Ahmed, J. Zhang, G. Rizzoni, and H. He, "Structural analysis based sensors fault detection and isolation of cylindrical lithium-ion batteries in automotive applications," *Control Engineering Practice*, vol. 52, pp. 46–58, 2016.

[43] M. J. Daigle and C. S. Kulkarni, "Electrochemistry-based battery modeling for prognostics," 2013.

[44] A. L. Dulmage and N. S. Mendelsohn, "Coverings of bipartite graphs," *Canadian Journal of Mathematics*, vol. 10, pp. 517–534, 1958.

[45] E. Frisk, A. Bregon, J. Aslund, M. Krysander, B. Pulido, and G. Biswas, "Diagnosability analysis considering causal interpretations for differential constraints," *IEEE Transactions on Systems, Man, and Cybernetics-Part A: Systems and Humans*, vol. 42, no. 5, pp. 1216–1229, 2012.

[46] M. Krysander, E. Frisk, I. Lind, and Y. Nilsson, "Diagnosis analysis of modelica models," *IFAC-PapersOnLine*, vol. 51, no. 24, pp. 153–159, 2018.

[47] M. Krysander, J. Åslund, and M. Nyberg, *An efficient algorithm for finding over-constrained sub-systems for construction of diagnostic tests*. Linköpings universitet, 2005.

[48] M. Krysander, J. Aslund, and M. Nyberg, "An efficient algorithm for finding minimal overconstrained subsystems for model-based diagnosis," *IEEE Transactions on Systems, Man, and Cybernetics-Part A: Systems and Humans*, vol. 38, no. 1, pp. 197–206, 2007.

[49] C. Svärd, M. Nyberg, and E. Frisk, "A greedy approach for selection of residual generators," in *Proceedings of the 22nd International Workshop on Principles of Diagnosis (DX-11)*, 2011.

[50] C. Svard, M. Nyberg, and E. Frisk, "Realizability constrained selection of residual generators for fault diagnosis with an automotive engine application," *IEEE Transactions on Systems, Man, and Cybernetics: Systems*, vol. 43, no. 6, pp. 1354–1369, 2013.

[51] J. Lunze, S. Pröll, and F. Jarmolowitz, "From structural analysis to observer-based residual generation for fault detection," in *2016 3rd Conference on Control and Fault-Tolerant Systems (SysTol)*. IEEE, 2016, pp. 491–498.

[52] S. Pröll, F. Jarmolowitz, and J. Lunze, "A comprehensive observer-based fault isolation method with application to a hydraulic power train," *IFAC-PapersOnLine*, vol. 49, no. 11, pp. 547–554, 2016.

[53] L. Petzold, "Differential/algebraic equations are not odes," *SIAM Journal on Scientific and Statistical Computing*, vol. 3, no. 3, pp. 367–384, 1982.

[54] C. W. Gear and L. R. Petzold, "Ode methods for the solution of differential/algebraic systems," *SIAM Journal on Numerical analysis*, vol. 21, no. 4, pp. 716–728, 1984.